[American Journal of Science, Vol. 313, April, 2013, P. 345–394, DOI 10.2475/04.2013.04]

COUNTRY ROCK MONAZITE RESPONSE TO INTRUSION OF THE SEARCHLIGHT PLUTON, SOUTHERN NEVADA

JOHN C. AYERS, SCOTT CROMBIE, MIRANDA LOFLIN, CALVIN F. MILLER, and YAN LUO

Department of Earth and Environmental Sciences, Vanderbilt University, Nashville, Tennessee 37027

ABSTRACT. We investigated how monazite grains in country rocks responded to the intrusion of the Miocene Searchlight pluton in southern Nevada. Country rock samples were collected from the roof zone and along transects on the flanks (wallrock) of the 16 to 17 Ma pluton. Deep wallrock Ireteba granite monazite grains have patchy secondary growth zones of Searchlight age overprinting primary growth zones of Ireteba age (~66 Ma). Shallow wallrock Proterozoic gneiss zircon grains define a discordia with an upper intercept age of 1.74 ± 0.02 Ga corresponding to crystallization of the protolith. Proterozoic gneiss monazite grains define a discordia with an upper intercept age of 1.64 ± 0.02 Ga and a poorly-defined lower intercept age of 75 ± 61 Ma that may correspond to the Ireteba intrusion. EMP analyses show that patchy secondary zones in Proterozoic gneiss monazite grains were contemporaneous with intrusion of the Ireteba granite, not the Searchlight pluton. Oxygen isotopes in Ireteba monazite, hydrogen and oxygen isotopes in whole rocks from the Ireteba transect, and oxygen isotopes in whole rocks from the Proterozoic gneiss transect show no systematic pattern related to the contact. No geochemical data support the hypothesis that hydrothermal fluids associated with intrusion of the Searchlight pluton caused monazite in the Proterozoic gneiss or Ireteba granite wallrock to partially recrystallize. Ireteba samples with the most intensely altered monazite were at the greatest paleodepths at the time of Searchlight intrusion and are the most deformed, suggesting that strain caused Ireteba monazite grains to partially recrystallize. In Proterozoic gneiss country rock monazite grains are present on the flanks but absent from the roof zone, suggesting that high fluid fluxes in the roof may have destroyed monazite. Strong focusing of hydrothermal fluid and heat into the roof zone prevented the development of a well-defined contact metamorphic aureole in Ireteba granite and Proterozoic gneiss wallrocks.

Key words: Monazite, zircon, geochronology, contact metamorphism, hydrothermal fluid, stable isotopes

INTRODUCTION

Monazite is a light rare earth element (LREE) phosphate that readily incorporates Th and U into its crystal structure while excluding Pb, making it a prime candidate for geochronology. The current explosion of interest in monazite and its widespread use in geochronology is primarily a result of advances in analytical instrumentation. Development of new instruments for isotopic dating of monazite such as SIMS (Quidelleur and others, 1997) and LA-ICP-MS (Paquette and Tiepolo, 2007) and new methodologies for chemical dating of monazite using existing instruments such as the electron microprobe (Williams and others, 1999) and XRF (Engi and others, 2002) have prompted many studies that have highlighted the unique utility of monazite for dating specific types of geologic events. However, the interpretation of in-situ monazite ages is complicated because monazite can grow in a variety of ways and commonly displays complex internal zoning, and no accepted criteria exist for correlating internal growth zones with specific growth mechanisms.

Corresponding author: john.c.ayers@Vanderbilt.Edu

In their review of the paragenesis of monazite Spear and Pyle (2002) noted that monazite growth or recrystallization can occur in response to changes in pressure and temperature (heterogeneous reaction), strain, fluid influx (dissolution/reprecipitation), annealing (Ostwald ripening), and precipitation from a fluid. Monazite may form during prograde metamorphism, and due to its high closure temperature for the U,Th-Pb systems it can preserve its primary crystallization age through peak metamorphism (Copeland and others, 1988; Smith and Barreiro, 1990; Kingsbury and others, 1993; Harrison and others, 2002). Monazite may also record events during retrograde metamorphism (Ayers and others, 2002; Gordon and others, 2009). Metamorphic zircon grains commonly record a narrow range of ages corresponding to one metamorphic event generally interpreted to represent near-peak metamorphism, whereas metamorphic monazite ages can span a larger range, often being younger but sometimes older than zircon ages.

Another aspect of monazite that distinguishes it from zircon is its greater tendency to recrystallize partially or completely in the presence of fluids, resulting in "patchy" zoning, a shift in oxygen isotope composition, and partial or complete resetting of the U,Th-Pb systems (Ayers and others, 2006; Bosse and others, 2009). Thin rims of monazite (and zircon) can also grow on pre-existing grains in response to fluid activity, as revealed by SIMS depth profiling (Gordon and others, 2009). These characteristics make monazite useful for identifying and dating fluid events. In plutonic settings where country rocks such as quartzo-feldspathic gneiss or granite are relatively unaffected by hydrothermal alteration, monazite may be the only useful indicator of fluid infiltration.

In this study we tested the hypothesis of Townsend and others (2000) that patchy secondary zones in monazite grains from the Ireteba granite formed in response to infiltration of hydrothermal fluids associated with intrusion of the Searchlight pluton in southern Nevada. We expanded the scope of the study to include monazite grains from Proterozoic gneisses in the Searchlight country rock that also display patchy zoning. We used geochronology and stable isotopes in an attempt to evaluate a possible link between Searchlight-associated hydrothermal fluids, which formed extensive hydrothermal ore deposits above the Searchlight pluton, and monazite alteration in country rocks.

Hydrothermal Alteration of Monazite

Hydrothermal alteration of monazite is an important process because it disturbs the monazite U,Th-Pb systems (Poitrasson and others, 2000; Mathieu and others, 2001). This creates the potential to date hydrothermal alteration events. Monazite has been used to date hydrothermal alteration events in a contact metamorphic aureole (Ayers and others, 2006), a migmatite dome (Gordon and others, 2009), pegmatite veins (Bosse and others, 2009), and multiple gold mineralization events in Australia (Rasmussen and others, 2006; Rasmussen and others, 2007).

As noted by Harrison and others (2002), radiogenic lead can be lost through diffusion, dissolution-reprecipitation or recrystallization. Diffusive Pb loss can cause individual growth zones to become discordant; however, this is presumably rare because the diffusivity of Pb in monazite is very low, resulting in very high closure temperatures (Cherniak and others, 2004; McFarlane and Harrison, 2006). In contrast, dissolution-reprecipitation and recrystallization result in loss of all radiogenic Pb, causing complete resetting of the affected growth zones (Williams and others, 2011). Although strain-induced recrystallization is responsible for monazite resetting in a few cases (Getty and Gromet, 1992), dissolution-reprecipitation in the presence of an aqueous fluid is considered to be the most common resetting mechanism (Harlov and Hetherington, 2010; Harlov and others, 2011).

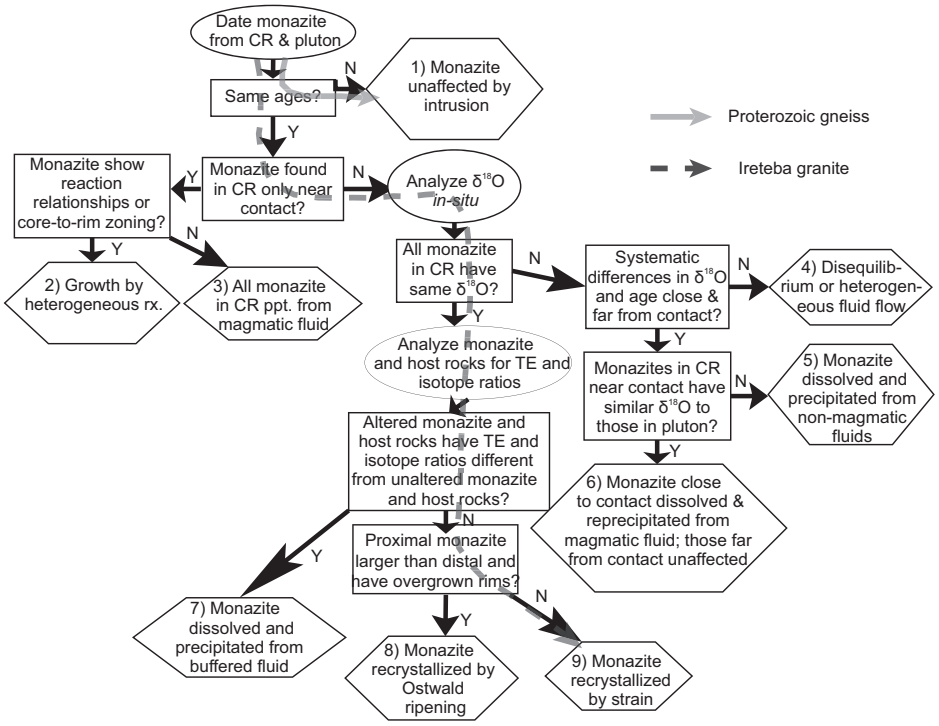

Fig. 1. Flow chart illustrating approach to identifying monazite growth mechanism. Diagram assumes that CR = Country Rock was one homogeneous unit prior to intrusion. Abbreviations: ppt = precipitation, rx = reaction.

Alteration and Resetting of Monazite in Contact Metamorphic Aureoles

Because monazite can grow, recrystallize, and alter in a variety of ways, it can be used to date many different types of processes. We chose to characterize the response of monazite to metamorphic and/or fluid events by focusing on country rock associated with magma intrusion and fluid exsolution at upper crustal conditions for the following reasons: contact metamorphic zones have better geologic control than regional metamorphism (small scale, simple geometry); unmetamorphosed protoliths are commonly available for comparison with metamorphosed equivalents; transects allow evaluation of effects of continuous changes in metamorphic grade and alteration intensity; fluid fluxes and peak temperatures vary systematically in relation to the contact; and monazite alteration has previously been demonstrated in such settings. Plutons act as sources of heat and volatiles that can alter and isotopically reset monazite in country rock. Characterizing the response of monazite to a well-defined, discrete event (magma intrusion) allows refinement of interpretations of monazite ages in less well-defined settings. Figure 1 illustrates our approach for distinguishing nine possible responses of monazite in country rocks to intrusion.

The ideal geometry for characterizing the effect of magmatic intrusion on country rocks is a planar contact; linear traverses from the contact into country rock allow evaluation of the effect of continuously decreasing intensity of metamorphism and fluid flux on texture and trace element and isotopic composition of monazite and its host rock. Carson and others (2002) used this approach to evaluate the effects of fluids derived from a pegmatite vein on the zircon U-Pb system along a traverse perpendicular to the vein contact.

Several recent studies document the effect of contact metamorphism on monazite. Ayers and others (2006) studied the response of monazite in Cambrian quartzite country rock to the intrusion of the Birch Creek granite. They found that monazite grains ~0.5 km from the contact experienced moderate- to low-temperature alteration by F-rich magmatic fluids, resulting in patchy zoning and $\delta^{18}O$ and Th-Pb ages similar to monazite grains in the pluton. In contrast, monazite grains in samples ~0.6 km from the contact and outside of the mapped hydrothermal zone show concentric zoning and $\delta^{18}O$ and Th-Pb ages very different from monazite grains in the pluton. Ayers and others (2006) suggested that monazite grains within the hydrothermal alteration zone dissolved and reprecipitated during magmatic fluid infiltration (mechanism #6 in fig. 1), while monazite grains outside of the zone were unaffected.

Other researchers also find an important role for fluids during growth/recrystallization of monazite in contact metamorphic aureoles. For example, Rasmussen and Fletcher (2002) documented the low-temperature growth of monazite in carbonaceous shales in response to intrusion of dolerite sills and associated hydrothermal fluid infiltration, which opens up the prospect of dating mafic intrusions that have no dateable minerals. Rasmussen and others (2001) demonstrated that monazite can precipitate from low-temperature, oxidizing hydrothermal fluids in the aureoles of granitic intrusions. Both studies attributed monazite growth to fluid mobilization and precipitation of REE.

In the studies of Ayers and others (2006), Rasmussen and Fletcher (2002), and Rasmussen and others (2001), monazite grains in country rock close to the intrusion yield one age, the age of intrusion. However, in some settings in-situ dating of monazite in country rocks yields more than one age (Townsend and others, 2000), and in many settings it is not clear what process produced or reset the dated monazite, which hampers interpretation of measured ages.

We used previously collected samples of the Ireteba granite (country rock of the Searchlight pluton) along with new samples collected along transects from the contact into Ireteba granite and Proterozoic gneiss country rock to test the hypothesis of Townsend and others (2000) that hydrothermal fluids were responsible for the partial recrystallization (through dissolution-reprecipitation) of monazite in the Searchlight aureole, and to see if monazite can be used to identify and date fluid infiltration events even in rocks that lack evidence of intense hydrothermal alteration. We also measured the stable isotope compositions of whole rocks collected along transects to look for evidence of fluid infiltration and to possibly identify the source of the fluid. Our primary objectives were to characterize the response of pre-existing monazite to the intrusion of an igneous body, to seek evidence of fluid infiltration into the country rocks of the Searchlight intrusion, and to identify the geologic processes associated with monazite ages measured *in-situ*.

BACKGROUND AND GEOLOGICAL SETTING

The study area is in the southern Eldorado and northernmost Newberry Mountain ranges in southeastern Nevada. It is part of a large west-tilted fault block within the northern Colorado River Extensional Corridor, a 50 to 100 km wide extensional belt that experienced peak extension and magmatism at ~16 to 15 Ma (Faulds and others, 1990). Miocene age volcanic and sedimentary strata are exposed along the western edge of these fault blocks (Bachl and others, 2001; Faulds and others, 2001; Faulds and others, 2002). Volcanic rocks range in composition from rhyolite to basalt (Faulds and others, 2002). Basement rocks consist mainly of Proterozoic granites and meta-igneous and meta-sedimentary gneisses intruded by intermediate to felsic plutonic rocks that are coeval with the volcanic strata (fig. 2) (Bachl and others, 2001; Perrault, ms, 2006). First we describe the Searchlight pluton, and then the Ireteba granite and Proterozoic gneiss country rocks that it intruded and metamorphosed.

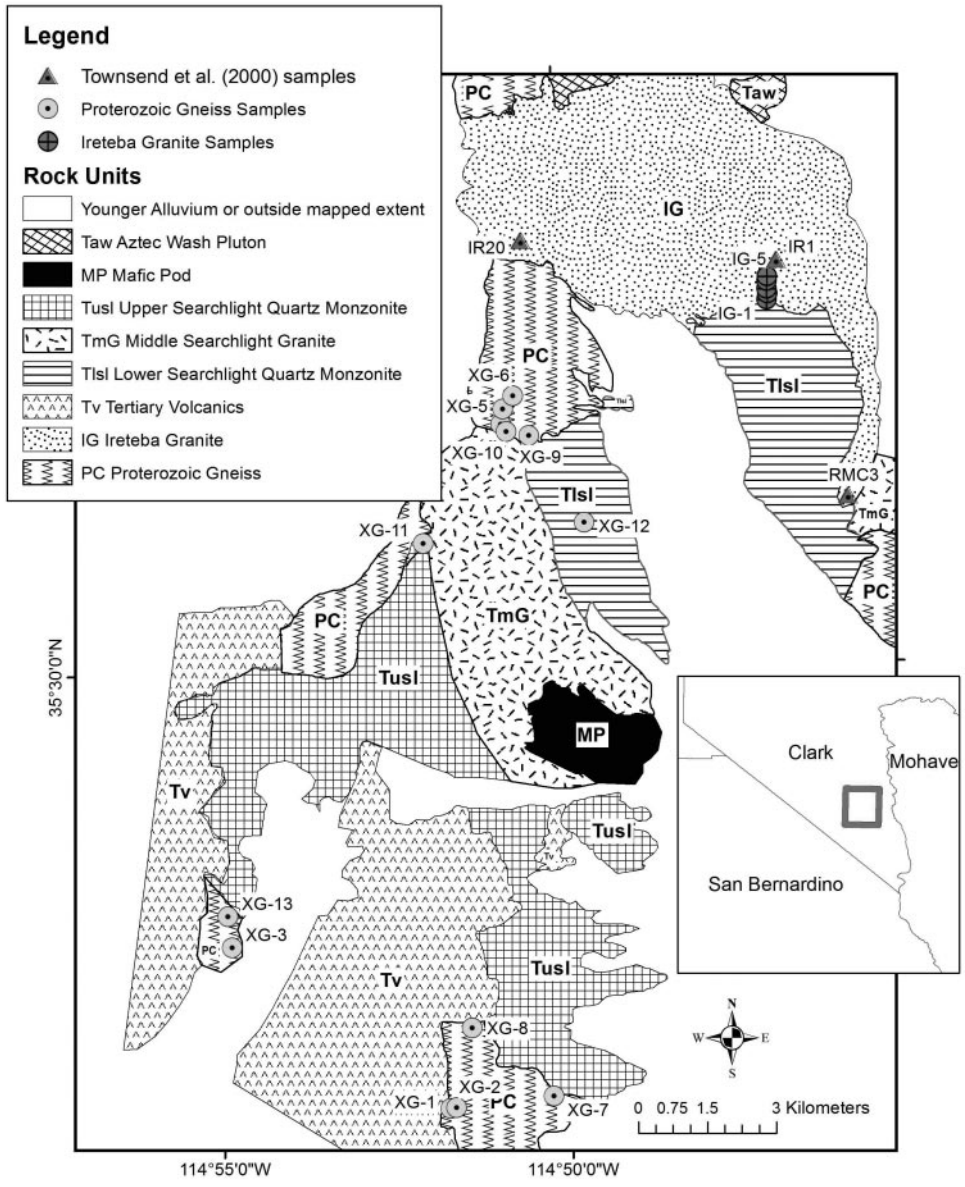

Fig. 2. Geologic map of Searchlight pluton and country rocks showing sample locations, after Bachl (2001) and Perrault (ms, 2006). Samples IR1, IR20, and RMC3 collected and described by Townsend and others (2000). Inset location map labelled with county names.

Searchlight Pluton

The Searchlight pluton is part of a large west-dipping block in the footwall of the Dupont Mountain fault (Bachl and others, 2001). Tilting has exposed this pluton in cross section with the shallow levels exposed to the west and the deeper levels of the pluton exposed in the east (Bachl and others, 2001). The upper Searchlight pluton is a fine- to medium-grained quartz monzonite (63-71 wt.% SiO_2), the middle Searchlight

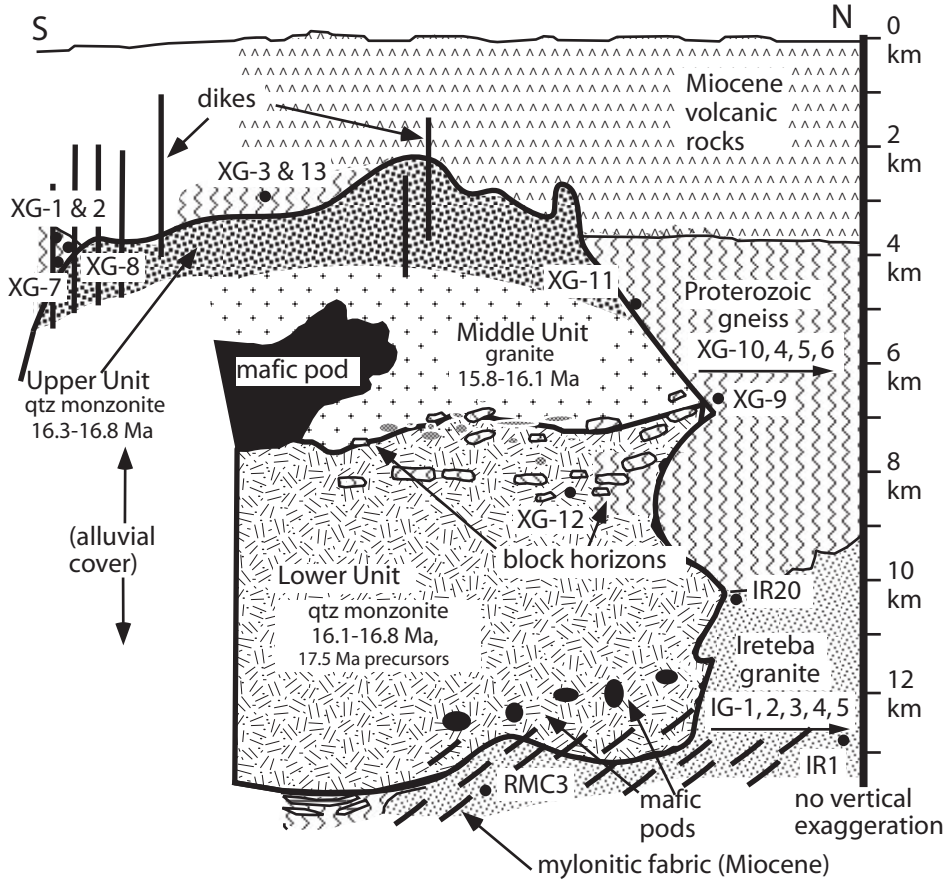

Fig. 3. Schematic cross section, with no vertical exaggeration, of the Searchlight pluton after emplacement (modified from Bachl and others, 2001). Sample locations for this study are filled circles with sample labels.

is a medium-grained granite (69-78 wt.% SiO_2), and the lower Searchlight is a coarse-grained quartz monzonite (59-70 wt.% SiO_2) (Bachl and others, 2001). Measurements of crystallization depth by aluminum-in-hornblende barometry suggest an initial depth for the roof of the pluton at 3 km and the floor at 13 km (Bachl and others, 2001). The Highland Range Volcanic Sequence is believed to be the volcanic counterpart of the Searchlight intrusion (Faulds and others, 2001, 2002; Colombini and others, 2011).

Zircon geochronology documents an approximately two million year history for the Searchlight pluton, with ages ranging from 15.8 to 17.7 Ma (Cates and others, 2003; Means and others, 2003; Miller and others, 2003). Most of the pluton, however, appears to have crystallized in the interval 16.8 to 15.8 Ma. To the southwest the upper pluton contacts both Proterozoic augen gneisses and Miocene volcanic rocks. A moderately irregular contact with the ~66 Ma Ireteba granite bounds the deeper portions, with re-entrants of up to 200 to 300 m. Felsic dikes from the lower unit penetrate the Ireteba granite up to several hundred meters, with contacts in outcrop appearing razor-sharp (Bachl and others, 2001). Figure 3 is a schematic cross-section of the pluton after emplacement. Deformation during and after Search-

light intrusion led to the development of a mylonite zone in the lowermost Searchlight and the deeper parts of the Ireteba granite that were originally beneath the Searchlight pluton.

Intrusion of the Searchlight pluton led to the formation of extensive hydrothermal deposits of Cu, Au, and Ag in its roof zone. More than 420,000 tons of ore were mined from the Searchlight district between 1902 and 1934 (Callaghan, 1939; Ludington and others, 2005; Lledo and Cline, 2008). Much of the important hydrothermal ore deposits occur in the roof zone of the upper Searchlight pluton where it intrudes the Miocene volcanic sequence (Callaghan, 1939). The overlying Miocene volcanic sequence is roughly 3 km thick, consistent with depth estimated by aluminum-in-hornblende barometry and supporting interpretation of Searchlight pluton as a magma chamber or series of chambers that underlay a volcano (fig. 3; Faulds and others, 2002, 2008). Remnants of Proterozoic gneiss in the roof zone host abundant quartz-rich, ore-bearing veins that are genetically related to the Searchlight pluton (Callaghan, 1939). The uppermost Searchlight pluton is largely unaltered, but overlying Miocene volcanic rocks in the roof zone show evidence of intense alteration including oxidation (Ludington and others, 2005; Lledo and Cline, 2008). The volcanic sequence is altered only where it overlies the Searchlight pluton.

Ireteba Granite

Miocene tilting has also provided a cross section of the ~66 Ma Ireteba pluton, with the shallowest levels to the west and deeper levels to the east (Townsend and others, 2000; Kapp and others, 2002). The current exposures of the pluton were ~5 to 13 km deep when the Searchlight pluton was emplaced at 17 to 16 Ma (Townsend and others, 2000). The Ireteba is a two-mica granite composed of plagioclase, quartz, K-feldspar, biotite, muscovite, accessory minerals, and locally garnet (Kapp and others, 2002). Zircon rim ages yielded an average $^{206}Pb/^{238}U$ age of 66.5 ± 2.5 Ma (Kapp and others, 2002). Along the southern margin of the pluton the shallow levels are in contact with Proterozoic gneiss and the deeper portions contact the 16.8 Ma Lower Searchlight quartz monzonite, while the northern border of the pluton is in contact with the 15.8 to 15.6 Ma Aztec Wash pluton (Cates and others, 2003). The western portion of the Ireteba pluton is undeformed. A dominantly linear, ductile strain fabric appears and increases in intensity toward the southeastern (deeper) part of the pluton. A band of highly deformed mylonitic granite extends south from the southeast corner of the main Ireteba body, east of Searchlight pluton, and underlies the east-dipping, brittle Dupont fault (figs. 2 and 3) (Kapp and others, 2002). Evidence of low-temperature fluid alteration includes minor sericitization of plagioclase, chlorite replacement of biotite, and minor quartz veins and vugs, suggesting that the fluid/rock ratio was low.

Townsend and others (2000) identified a bimodal age distribution in Ireteba monazite grains with peaks at 64 and 16 Ma (Kapp and others, 2002). Ion microprobe (IMP) Th-Pb monazite dating of shallow samples yielded 65 to 60 Ma ages for magmatic and some replacement zones in monazite, while crosscutting secondary zones that have a vein-like appearance yielded ages as young as Miocene (Townsend and others, 2000). Monazite from deeper samples yielded a few 65 to 55 Ma ages for remnant magmatic zones and abundant Miocene ages for replacement zones (~16 Ma) that displayed patchy zoning (Townsend and others, 2000). The ~16 Ma ages were interpreted to result from the dissolution-reprecipitation of select monazite zones by fluids released during the emplacement and cooling of the adjacent Miocene Searchlight and Aztec Wash plutons (Townsend and others, 2000). Although Townsend and others (2000) clearly showed that portions of monazite grains in the Ireteba granite recrystallized and reset at approximately the same time as the intrusion of the Searchlight pluton, and that the secondary replacement zones commonly display

patchy zoning, the role of hydrothermal fluids and the extent to which the Searchlight intrusion may have altered other country rock in the area remain unclear. Oxygen isotopic compositions of the Ireteba and Searchlight plutons do not overlap [Ireteba $\delta^{18}O$ 8.2-8.8‰ (Townsend, ms, 1999; Townsend and others, 2000; Kapp and others, 2002), Searchlight $\delta^{18}O$ 7.0, 7.1‰ (Bachl and others, 2001)], so if a Searchlight-associated fluid infiltrated the Ireteba it could have caused distinct changes in oxygen isotope composition of whole rocks and Ireteba monazite grains.

Proterozoic Gneiss

Proterozoic gneiss country rocks are part of the Paleoproterozoic Mojave province. The oldest known rocks of the Mojave province are approximately 1.8 Ga metasedimentary rocks, but detrital and inherited zircon ages and whole-rock Nd and Pb isotope data demonstrate contributions from 2.8 to 1.8 Ga sources (Bennett and DePaolo, 1987; Strickland and others, 2013). Gabbroic to granitic magmas (now gneiss) crystallized at ~1.76 Ga, followed by high-grade metamorphism and emplacement of leucogranites at 1.74 Ga, and intrusion of granites and some gabbros and metamorphism during the 1.72 to 1.70 Ga Ivanpah orogeny (Wooden and Miller, 1990). After peak orogeny abundant intermediate to felsic magmas intruded the eastern Mojave between 1.69 and 1.62 Ga, with a final metamorphic event at ~1.67 Ga (Wooden and Miller, 1990). Strickland and others (2013) report episodes of monazite growth in Mojave province rocks of the Ivanpah Mountains, 50 km west of the Searchlight area, at 1.74 and 1.67 Ga.

At 1.45 to 1.40 Ga abundant granitic magma intruded the eastern Mojave crust to form part of the ca. 1.4 Ga "anorogenic" granite belt that transects North America (Anderson, 1989; Miller and Wooden, 1994). Intrusion of diabase dikes and sills at 1.1 Ga marked the last Proterozoic event recorded in the eastern Mojave (Hammond and Wooden, 1990). Proterozoic exposures in the Searchlight area primarily consist of gneisses. The southern and northern portions of the roof zone (see fig. 2) are chiefly augen orthogneiss, comprising strained, polycrystalline quartz, highly altered plagioclase, potassium feldspar phenocrysts (now augen), secondary muscovite, biotite, chlorite, opaques, zircon, apatite, and crosscutting epidote-rich veins. The northern wall zone (fig. 2) is a complex zone of biotite- and sometimes garnet-rich paragneiss, interleaved with orthogneiss, leucogranite that can be garnet-rich, and minor amphibolite.

Sample Descriptions

Detailed sample descriptions are given in Crombie (ms, 2006). Five samples of the Ireteba granite were collected along a 0.9 km north-trending transect perpendicular to the lower Searchlight-Ireteba contact (figs. 2 and 3, table 1). The Ireteba samples are all strained (lineated and foliated) leucogranites and show little textural or mineralogical evidence of alteration, with minor sericitization of plagioclase and replacement of biotite by chlorite.

While the lithologies of the Proterozoic gneisses are highly variable, sample collection focused on those rocks most likely to contain monazite, that is, rocks with peraluminous mineralogy. Samples of the Proterozoic gneiss were collected along a 0.5 km transect northward from the northern flank of the Searchlight pluton into the country rock (XG-10, XG-4, XG-5, and XG-6), in the wallzone close to the contact (XG-9 and XG-11), from a large block in the lower Searchlight zone (XG-12), and from the roof zone above the Searchlight pluton (XG-1, XG-2, XG-3, XG-7, XG-8, XG-13) (figs. 2 and 3, table 1). No monazite grains were found in XG-1, XG-3, XG-8, and XG-13, so we will not discuss them further.

TABLE 1

Whole rock major and trace element compositions of samples

Sample	IG-1	IG-2	IG-3	IG-4	IG-5	XG-10	XG-4	XG-5	XG-6	XG-2	XG-7	XG-9	XG-11	XG-12
	Ireteba Granite transect					Proterozoic Gneiss transect				Roof		Wall		Block
SiO_2[a]	75.3	75.1	74.4	72.5	75.0	63.5	75.0	73.4	73.1	67.7	59.6	66.3	71.2	61.6
Al_2O_3[a]	13.8	14.2	14.9	16.1	14.5	16.7	12.9	14.7	14.7	13.8	16.8	13.8	14.2	17.8
Fe_2O_3[a,b]	0.87	0.91	0.90	0.85	0.90	7.75	4.04	0.61	3.49	4.64	6.92	8.28	3.81	6.20
MnO[a]	0.01	0.02	0.02	0.06	0.06	0.09	0.14	0.02	0.04	0.08	0.12	0.14	0.03	0.06
MgO[a]	0.17	0.19	0.18	0.13	0.14	2.53	0.93	0.17	0.77	1.83	3.36	2.75	1.49	2.30
CaO[a]	1.4	1.6	1.7	0.9	1.5	0.2	2.1	0.7	1.4	4.8	5.4	1.8	1.2	2.1
Na_2O[a]	3.7	4.2	4.4	4.4	4.4	1.3	2.5	2.4	2.9	4.1	4.3	2.7	2.6	3.2
K_2O[a]	4.7	3.7	3.5	4.9	3.5	6.9	2.0	7.9	3.0	2.0	2.1	3.2	4.9	5.8
TiO_2[a]	0.07	0.08	0.06	0.05	0.05	1.00	0.26	0.01	0.48	0.76	1.04	1.03	0.45	0.93
P_2O_5[a]	0.05	0.05	0.05	0.05	0.04	0.04	0.05	0.09	0.08	0.26	0.46	0.07	0.06	0.08
LOI	0.52	0.55	0.51	0.44	0.73	1.76	0.9	0.37	1.06	2.6	1.08	0.99	0.79	0.74
Total[c]	99.8	99.9	99.7	99.8	99.2	99.2	99.7	99.7	99.9	99.5	99.9	100.0	99.5	99.5
A/CNK[d]	1.02	1.04	1.06	1.14	1.07	0.78	1.26	1.07	1.38	0.88	1.24	1.67	1.21	1.16
A/NK[d]	1.25	1.32	1.35	1.29	1.32	1.75	2.02	1.17	1.82	1.56	1.81	1.74	1.49	1.54
Sc	< 1	2	2	4	2	18	21	3	5	9	13	21	16	16
V	11	< 5	6	< 5	< 5	119	11	< 5	39	71	104	125	56	115
Cr	< 20	< 20	< 20	< 20	< 20	90	< 20	< 20	30	40	80	80	40	80
Co	< 1	< 1	< 1	< 1	< 1	14	4	< 1	5	7	14	15	5	8
Ni	< 20	< 20	< 20	< 20	< 20	30	< 20	< 20	< 20	< 20	40	40	< 20	20
Zn	< 30	< 30	< 30	60	30	60	< 30	< 30	50	< 30	60	70	< 30	30
Ga	13	13	13	16	14	26	13	10	15	15	17	17	14	17
Rb	73	55	64	111	79	138	68	135	72	32	44	153	133	159
Sr	511	492	479	162	383	136	224	267	200	502	775	153	248	483
Y	5.2	3.8	6	14.7	5.8	25.4	78.4	10.5	12.4	11.9	16.6	49.1	49.5	46.8
Zr	62	62	43	31	36	253	391	22	156	159	179	297	230	293
Nb	1.9	2.7	2.8	5.7	3.6	18	8	0.7	9.5	10.5	10.6	15.5	8.8	12.3
Sb	0.9	0.9	0.9	1	0.7	1.1	0.7	0.8	1.3	1.1	1	0.9	0.6	1
Cs	0.4	0.4	0.4	0.5	0.4	3.7	1.1	3.8	1.3	0.3	1	3.7	4	3.8
Ba	1406	1413	1218	593	1099	1306	517	1698	793	555	1213	418	1182	2310
La	16	12.2	11.7	10.6	6.46	45	63	25	53	59	34	70	52	51
Ce	30	23.3	23	22.8	12.4	88	131	34	104	110	78	146	101	100
Pr	3.4	2.7	2.7	2.9	1.4	10	16	2.9	12	12	10	17	12	12
Nd	11	9.2	9.2	11.3	4.8	36	59	8.0	41	37	35	61	40	40
Sm	2.0	1.5	1.7	2.6	1.1	5.9	12	0.92	6.2	5.2	6.2	11.1	7.1	6.9
Eu	0.52	0.53	0.53	0.35	0.36	1.4	1.8	1.8	2.1	1.4	2.0	1.7	1.4	1.9
Gd	1.4	1.2	1.5	2.5	1.0	5.7	12.5	0.7	4.9	4.1	5.3	10.1	7	6.3
Tb	0.19	0.14	0.2	0.4	0.16	0.94	2.11	0.17	0.61	0.49	0.67	1.5	1.3	1.1
Dy	0.93	0.66	1.1	2.3	0.92	5.0	13	1.4	2.6	2.4	3.2	8.4	8.2	6.9
Ho	0.17	0.12	0.2	0.46	0.18	0.9	2.84	0.33	0.41	0.41	0.6	1.67	1.76	1.58
Er	0.5	0.37	0.55	1.38	0.57	2.39	9.15	1.09	1.0	1.1	1.6	5.03	5.48	4.98
Tm	0.08	0.06	0.08	0.22	0.10	0.31	1.46	0.17	0.12	0.16	0.22	0.74	0.84	0.82
Yb	0.51	0.44	0.54	1.45	0.69	1.84	9.42	1.11	0.65	0.99	1.37	4.61	5.38	5.29
Lu	0.08	0.07	0.08	0.21	0.11	0.27	1.36	0.15	0.09	0.14	0.19	0.69	0.77	0.77
Hf	2.2	2.1	1.5	1.6	1.6	7.4	11.3	1.1	4.6	4.3	4.5	8.4	6.8	8.6
Ta	0.32	0.1	0.11	0.14	0.15	0.93	0.39	0.19	0.68	0.77	0.49	0.95	0.49	0.67
Tl	0.32	0.29	0.34	0.56	0.47	0.89	0.38	0.74	0.44	0.19	0.34	1.01	0.6	0.99
Pb	22	22	20	26	27	11	15	43	20	10	15	14	6	50
Th	7.3	3.2	2.9	5.5	1.2	12	17	1.1	15	10	0.7	20	16	17
U	0.95	0.51	0.23	0.38	0.21	1.0	3.0	0.52	0.85	0.48	0.19	2.3	1.7	1.8

[a] Oxides in weight percent, normalized to 100% total.
[b] Total Fe as Fe_2O_3.
[c] Total oxides plus LOI prior to normalization.
[d] Rock is peraluminous if A/CNK = molar $(Al_2O_3/(2*CaO + Na_2O + K_2O))$ is > 1, and metaluminous if A/CNK < 1 and A/NK = molar $(Al_2O_3/(Na_2O + K_2O))$ is > 1.

METHODS

We cut each hand sample into two slabs, one for a standard petrographic thin section and the other for whole rock major and trace element and oxygen isotope analysis. We pulverized the slab for geochemical analyses in an alumina ceramic shatter box. Major and trace element and oxygen isotope analysis of whole rock powders of samples from the two transects were performed by Actlabs. Whole rock samples from the Ireteba granite transect were analyzed by Actlabs for hydrogen isotopes as well. We used the remainder of each sample for mineral separation.

Monazite was separated from samples using standard mineral separation techniques. Procedures in order of use included using a jaw crusher, rock pulverizer, water table, heavy liquids, and a Franz magnetic separator. Monazite was then hand-picked and mounted in 1 inch diameter epoxy rounds with 554 and 44069 monazite geochronology standards. We polished and carbon coated the mounts and then imaged grains using a Hitachi S-4200 Scanning Electron Microscope (SEM) at Vanderbilt University. We identified grains using an Energy Dispersive Spectrometer, and collected Back Scattered Electron (BSE) images of each grain. BSE images show micrometer-scale differences in brightness that correspond to changes in mean atomic number (composition). We used these images to guide our selection of analysis spots using Laser Ablation-Inductively Coupled Plasma-Mass Spectrometry (LA-ICP-MS) and Electron Microprobe (EMP).

LA-ICP-MS analysis was conducted at Vanderbilt University using a Perkin Elmer 6100 DRC ICP-MS coupled with a New Wave/Merchantek 213 nm Nd:YAG laser, and a mixture of He and Ar carrier gas. He carrier gas was flushed into the ablation cell and admixed with nebulizer argon ~30 cm behind the ablation cell. This mixture was then transported to the ICP-MS. Before each analysis session we warmed up the laser by firing at low power for one hour.

For LA-ICP-MS monazite geochronology we measured the following analytes in all sessions: ^{40}P, ^{139}La, ^{204}Pb, ^{206}Pb, ^{207}Pb, ^{208}Pb, ^{232}Th, ^{238}U, and ^{248}ThO. During the optimization process we fired the laser at NIST-610 glass using analysis settings (5 Hz, pulse energy density of ~11 J/cm^2, and a 30 μm spot size) and adjusted the rf-power, lens voltage, and nebulizer flow to increase sensitivity for each analyte and keep the ratio of Th/ThO lower than 0.5%. Unknown data were collected in groups of five analyses bracketed by analysis of external standards [554 monazite for ^{208}Pb/^{232}Th (Harrison and others, 1999) and 44069 monazite for ^{206}Pb/^{238}U and ^{207}Pb/^{235}U (Aleinikoff and others, 2006)]. After every fourteen analyses we re-analyzed NIST-610 glass. Each sample analysis lasted 100 s, with a 30 s background measurement during which the laser was not firing.

For LA-ICP-MS zircon geochronology we analyzed for ^{91}Zr, ^{204} Pb, ^{206} Pb, ^{207} Pb, ^{208}Pb, ^{232}Th, ^{238}U, and ^{248}ThO. We optimized the ICP-MS using continuous ablation of NIST 610 glass to provide maximum sensitivity of ^{208}Pb while maintaining low oxide formation ($ThO^+/Th^+ < 0.5\%$). We used NIST610 as an external standard for determination of concentrations of Ti, U and Th, and Harvard 91500 zircon as the external standard for geochronology (Wiedenbeck and others, 2004). Zirconium was the internal standard for determination of trace element concentrations. For each analysis we acquired background signals for 30 s and time-resolved analyte signals for 70 s. We rejected the first few seconds of each signal to avoid obtaining data from surface contamination. The analysis pattern was NIST610 2x, 91500 2x, 5–10 samples, and repeat. Spot size was 60 or 80 μm depending on the size of the zone being dated, and laser frequency was either 10 or 15 Hz.

For both monazite and zircon geochronology we transferred the raw LA-ICP-MS data to the GLITTER software package for reduction (Griffin and others, 2008). GLITTER calculates the relevant isotopic ratios and displays them as time-resolved

intensity traces (van Achterbergh and others, 2001). We then inspected the time-resolved signals and selected the most stable portions of the signal for integration. Common lead corrections calculated using the method of Andersen (2002) were generally negligible and so were ignored. Resulting isotope ratios and errors were exported to Microsoft Excel and the Isoplot add-in (Ludwig, 2000) was used to generate concordia plots and probability density plots and histograms. The Unmix routine in Isoplot was used to identify peaks in the age spectra and to estimate the proportions of age groups.

To check the accuracy of our LA-ICP-MS monazite age dates we analyzed secondary standards. From 32 analyses of 44069 monazite collected during two sessions using 554 monazite as a standard, we rejected two analyses as outliers and obtained a weighted average $^{208}Pb/^{232}Th$ age of 419.8 ± 4.2 Ma (95% conf. limits, mean square of weighted deviates (MSWD) = 1.9); the concordant $^{206}Pb/^{238}U$ age determined using ID-TIMS is 424.9 ± 0.4 Ma (Aleinikoff and others, 2006). We also compared $^{208}Pb/^{232}Th$ ages measured using LA-ICP-MS and previously measured using a Cameca ims 1270 IMP. IMP analysis of monazite BMJ-1 yielded a $^{208}Pb/^{232}Th$ age of 117 ± 1 Ma (Bryant and others, 2004). We collected eight analyses of monazite BMJ-1 and rejected one as an outlier; the remaining seven analyses yielded an average $^{208}Pb/^{232}Th$ age of 119.8 ± 4 Ma (95% conf. limits, MSWD = 7.9). We conclude that our LA-ICP-MS monazite age dates are accurate, although MSWD values are commonly high, suggesting either that samples were not homogeneous, or errors on individual analyses were underestimated.

In order to check the accuracy of our method for zircon U-Pb dating we performed eleven analyses of secondary standard AS3 during two sessions and obtained a weighted average $^{206}Pb/^{238}U$ age of 1097 ± 20 Ma (95% CL, MSWD = 5.4). The accepted value is 1099.0 ± 0.5 Ma (Paces and Miller, 1993). The average one sigma error on $^{206}Pb/^{238}U$ individual analyses of AS3 was 13 Ma, corresponding to a precision of ~1% RSD. We also performed three analyses of sample MW99-B-2 previously dated at 231 ± 5 Ma by IMP (Ayers and others, 2002) and obtained a weighted average $^{206}Pb/^{238}U$ age of 239 ± 5 Ma (95% CL, MSWD = 0.31).

Because the LA-ICP-MS spot size was often larger than growth domains visible in BSE images, we measured chemical ages of Proterozoic gneiss monazite grains using EMP chemical age dating, which has higher spatial resolution than LA-ICP-MS. Major element and trace element concentrations, and Th-U-Pb dates, of monazite were measured at Rensselaer Polytechnic Institute using a Cameca SX-100 EMP operating at 15 keV and 100 nA with a beam width of 5 um using the methods of Pyle and others (2005).

Oxygen isotope compositions of monazite from sample IR-1 of Townsend and others (2000) were measured in-situ using the Cameca ims1270 multi-collector IMP at UCLA using the methods of Ayers and others (2006). Spot size was ~15 × 20 μm in diameter. Conventional mass spectrometric oxygen isotope analysis of monazite standards was performed by Bruce Taylor of the Geological Survey of Canada using a conventional fluorination procedure (Clayton and Mayeda, 1963) followed by gas source mass spectrometric analysis. Measured conventional values of $\delta^{18}O$ for monazite standards were Brazil = 1.43 ± 0.08‰ and 554 = 7.54 ± 0.12‰ (all $\delta^{18}O$ values referenced to SMOW). Measurements of $^{18}O/^{16}O$ on the IMP were background-corrected. Periodic measurement of $^{18}O/^{16}O$ on a standard over the course of an analytical session showed no significant drift over time. However, measured values of $^{18}O/^{16}O$ changed after we changed mounts. Accurate measurements require that standards and samples be prepared in the same mount. We therefore used the average value of the correction factor CF determined by multiple measurements of standard 554 on the same mount during the same analytical session as the samples to correct the background-

corrected $^{18}O/^{16}O$ measured ratios of the samples according to: $(^{18}O/^{16}O)_{t,s} = (^{18}O/^{16}O)_{m,s}$*CF, where CF = $(^{18}O/^{16}O)_{t,std}/(^{18}O/^{16}O)_{m,std}$ and t = true, m = measured, s = sample, and std = standard. In a given session standards 554 and Brazil have nearly identical correction factors even though their respective ThO_2 concentrations of ~3.7 percent and ~6.8 percent are very different, suggesting that composition does not affect the value of $\delta^{18}O$ measured on the IMP. The overall precision of our measurements is ±0.1 permil based on multiple measurements of standards.

RESULTS

Ireteba Granite

The Ireteba granite (IG samples) is a peraluminous granite with 72 to 75 weight percent SiO_2 (table 1). Harker diagrams for IG samples show that concentrations of compatible elements (Ca, Mg, Fe, Ti, Al, Sr, Ba, LREE) decrease and incompatible elements (Rb, K), though scattered, increase with increasing SiO_2, as observed by Kapp and others (2002). Generally, samples have LREE concentrations 20–50 x chondrite, HREE concentrations 1.5–3.6 x chondrite, and lack Eu anomalies (fig. 4A). This combined with high Sr concentrations (fig. 4B) suggests a garnet-rich, feldspar-poor source (Kapp and others, 2002). However, IG-4 has a negative Eu anomaly and a higher concentration of HREE (~7 x chondrite), as well as higher Sr and Ba, suggesting significant fractionation after extraction from its source.

Whole rock $\delta^{18}O$ values for the five Ireteba granite samples range from 8.1 to 9.5 permil (table 2). This correlates well with four previously analyzed Ireteba granite samples with whole rock $\delta^{18}O$ values ranging from 8.2 to 8.8 permil (Townsend and others, 2000; Kapp and others, 2002). Whole rock δD values range from −87 to −98 permil (table 2). No correlation of whole rock $\delta^{18}O$ or δD values with distance from the Searchlight contact emerged (fig. 5).

BSE images show two main types of compositional zoning in monazite from all monazite-bearing samples collected in the Searchlight aureole. We interpret concentric zoning to be primary magmatic zoning, and secondary patchy zoning that overprints the primary concentric zoning to result from dissolution-reprecipitation or recrystallization of monazite (fig. 6). Interaction with hydrothermal fluids could cause dissolution-reprecipitation (mechanisms 5-7 in fig. 1), while heat (compare mechanism 8) or strain (mechanism 9) could cause recrystallization. Many monazite grains in this study have a combination of concentric and patchy zoning. All compositional zones have sharp contacts, suggesting that intra-grain chemical diffusion did not cause or modify the zonation.

All five samples of Ireteba granite yielded monazite. The monazite grains are anhedral, rounded to angular, and range from ~50 μm to ~200 μm in diameter (fig. 6). BSE images show some combination of secondary patchy and primary concentric (magmatic) zoning in monazite grains (Townsend and others, 2000). Monazite compositional zoning commonly results from the two coupled substitutions (Zhu and O'Nions, 1999):

$$REE^{3+} + P^{5+} \leftrightarrow Th^{4+} \text{ or } U^{4+} + Si^{4+} \text{ (huttonite)} \quad (1)$$

$$2REE^{3+} \leftrightarrow Th^{4+} \text{ or } U^{4+} + Ca^{2+} \text{ (brabantite)} \quad (2)$$

Zoning expressed as variable BSE intensity is negatively correlated with La x-ray intensity (fig. 6A) and positively correlated with Th x-ray intensity (fig. 6B). This means that zones that are bright in BSE images have relatively high Th and low La concentrations, as expected for brabantite and huttonite substitution. Monazite grains with only patchy zoning are most common in the collected samples. Because Townsend and others (2000) measured many IMP Th-Pb ages and correlated ages with zoning, we did

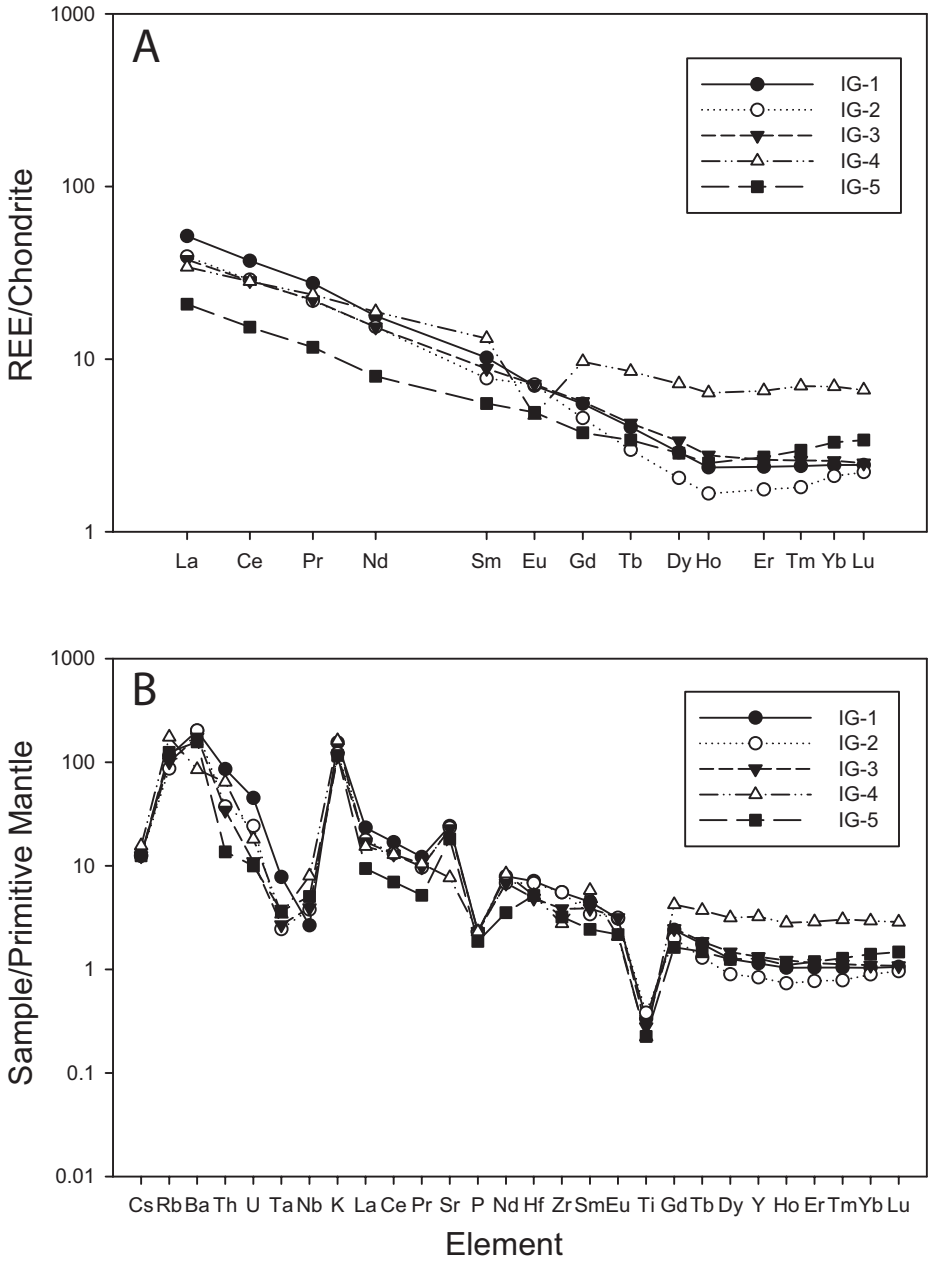

Fig. 4. Ireteba granite whole rock trace element compositions. (A) Chondrite normalized REE diagram. Chondrite values from Boynton (1984). (B) Concentrations normalized to primitive mantle (Sun and McDonough, 1989).

not place a high priority on dating Ireteba monazite grains. Although we measured monazite compositions using an EMP (table 3A), we did not measure EMP chemical ages of Ireteba monazite grains and did not record the locations of EMP or LA-ICP-MS analyses, so we cannot correlate the measured ages with internal zoning (the same is

TABLE 2

Distance from contact and whole rock isotope data for samples collected along transects

Sample	IG-1	IG-2	IG-3	IG-4	IG-5	XG-10	XG-4	XG-5	XG-6
Distance from contact (km)	0.000	0.095	0.195	0.364	0.462	0.013	0.044	0.337	0.671
$\delta^{18}O_{SMOW}$ (‰)	8.9	8.1	9.5	8.9	8.5	8.3	12.4	10.3	10.7
δD_{SMOW} (‰)	-94	-95	-87	-98	-94				
wt% H_2O	0.3	0.4	0.4	0.3	0.4				
Avg. $^{208}Pb/^{232}Th$ age (Ma)	18	38	50	21	35				
1 σ error	1	17	11	5	22				
Avg. $^{207}Pb/^{206}Pb$ age (Ma)*						1644	1663	1633	1663
1 σ error						34	43	120	23

* Used $^{207}Pb/^{206}Pb$ ages for XG samples because $^{208}Pb/^{232}Th$ ages not measured for XG-4.

Note: Distances of other samples from contact in km: XG-7 = 0.092, XG-1 = 0.093, XG-2 = 0.202, XG-12 = 0 (stoped block).

not true of analysis of XG monazite and zircon, see below). However, Townsend and others (2000) established that the primary magmatic zones yield Ireteba crystallization ages of near ~64 Ma and patchy secondary zones with high huttonite ($ThSiO_4$) component yield Searchlight ages of ~16 Ma. Likewise, our EMP analyses of monazite from sample IR1 show higher Th concentrations in secondary zones (table 3B).

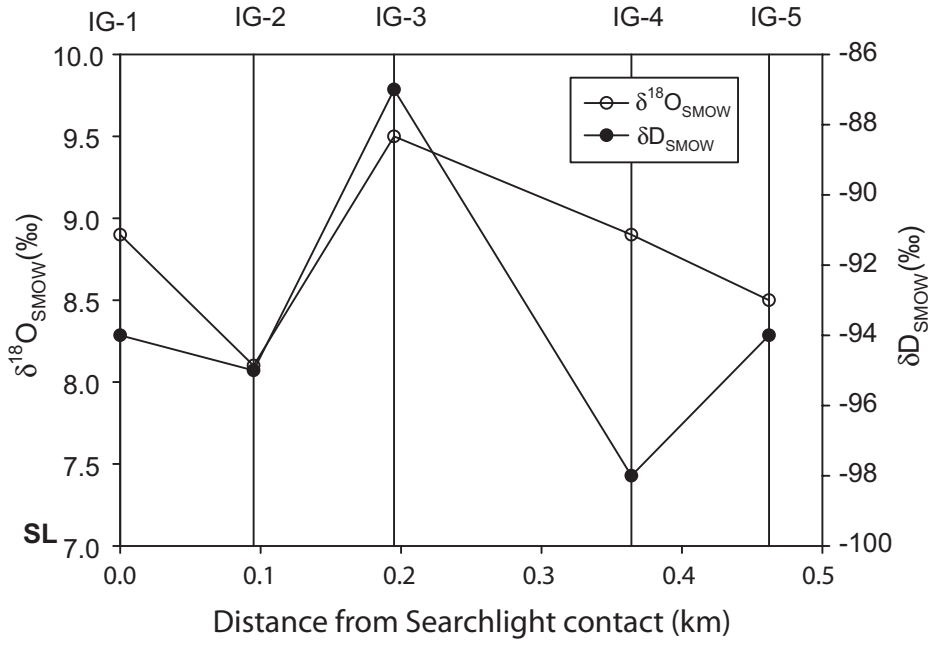

Fig. 5. Ireteba granite whole rock stable isotope compositions. $\delta^{18}O_{SMOW}$ (left y-axis) and δD_{SMOW} (right y-axis) are plotted as a function of distance from the Searchlight contact. "SL" indicates the average $\delta^{18}O_{SMOW}$ of two Searchlight pluton samples (Bachl and others, 2001).

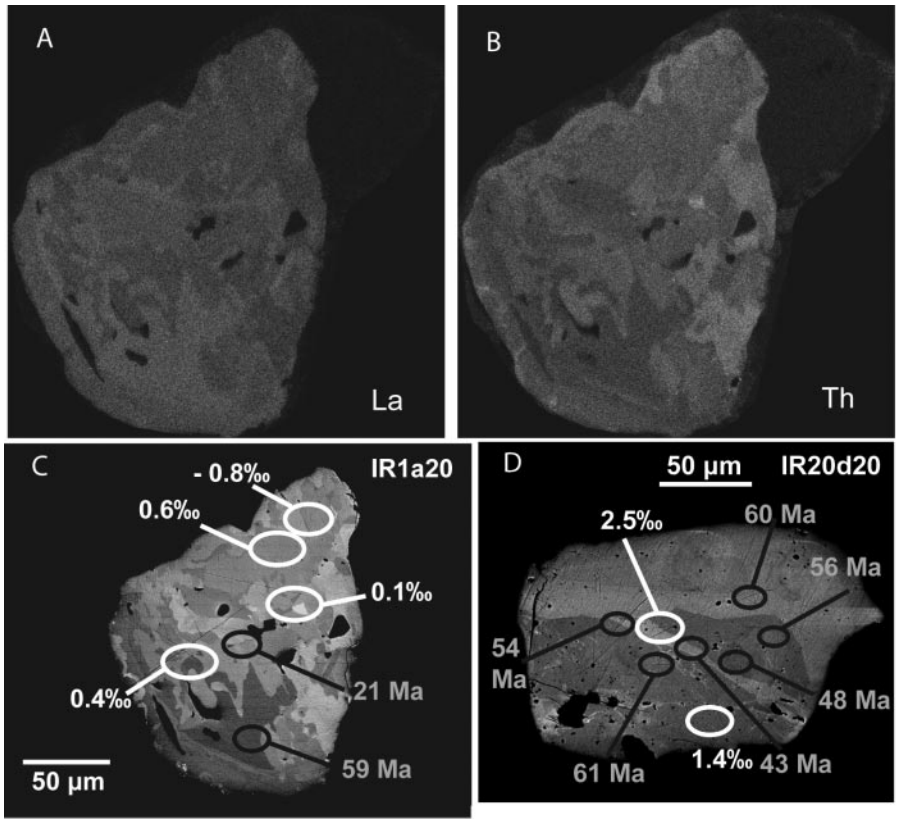

Fig. 6. Images of Ireteba monazite grains. (A) La x-ray map of grain IR1a20. (B) Th x-ray map of same grain. (C) Backscattered electron image of grain IR1a20. (D) Backscattered electron image of grain IR20d20. (C) and (D) are labelled with $^{208}Pb/^{232}Th$ IMP ages from Townsend and others (2000) and $\delta^{18}O_{SMOW}$ values from this study. Grain IR1a20 displays patchy zoning in secondary domain characteristic of Ireteba monazite grains that were at the greatest paleodepths in rocks that experienced ductile deformation.

LA-ICP-MS analysis of all Ireteba samples yields a bimodal $^{208}Pb/^{232}Th$ age distribution (table 4, fig. 7). Measured ages range from 15.1 Ma to 61.1 Ma with major peaks at ~19 and 54 Ma. The younger age peak is close to but older than the Searchlight crystallization age range (15.8-17.7 Ma, Faulds and others, 2002; Cates and others, 2003; Miller and others, 2003), while the older age peak is close to but younger than the 66 Ma age of the Ireteba granite (Kapp and others, 2002). The two age peaks in the bimodal distribution from our samples are similar to those obtained by Townsend and others (2000) when they included mixed analyses (labelled "all analyses" in fig. 7). This suggests that many if not most of our analyses were mixed analyses, particularly for the primary zones that were small and not abundant. Mixed analyses were common because we did not use BSE images to guide our choice of analysis spots and because our LA-ICP-MS has lower spatial resolution (spot size of 30 µm) than the IMP (15 × 20 µm).

We used the proportion of secondary (young) monazite as a proxy for alteration intensity. Although our choice of analysis spots was not random, samples with larger proportions of secondary monazite resulting from more extensive alteration yielded larger proportions of measured monazite $^{208}Pb/^{232}Th$ ages close to the 16 to 17 Ma age

TABLE 3A

Ireteba granite monazite compositions

Sample	IG-1	IG-2	IG-3	IG-4	IG-5
n	6	12	17	17	14
P_2O_5	27.8	27.5	29.9	28.1	28.7
SiO_2	0.95	2.38	0.26	1.1	1.0
ThO_2	3.3	3.1	2.6	4.3	4.8
Y_2O_3	1.2	1.2	1.8	2.6	2.4
La_2O_3	15.3	13.9	14.5	10.6	11.5
Ce_2O_3	30.7	29.2	29.7	24.9	26.6
Pr_2O_3	3.0	3.1	3.0	2.9	3.1
Nd_2O_3	10.8	11.8	11.6	12.5	12.9
Sm_2O_3	1.4	1.6	1.7	2.4	2.2
Gd_2O_3	1.0	1.1	1.3	2.2	1.9
Dy_2O_3	0.37	0.41	0.55	0.85	0.74
U_2O_3	0.11	0.10	0.05	0.13	0.16
CaO	0.70	0.55	0.95	0.88	0.85
Fe_2O_3	0.00	0.02	0.00	0.00	0.00
PbO	0.00	0.03	0.02	0.03	0.03
Total	**96.6**	**96.0**	**98.0**	**93.6**	**96.9**

of the Searchlight pluton. As expected, the sample average $^{208}Pb/^{232}Th$ age was lowest for sample IG-1 closest to the contact at 17.8 Ma and increased with increasing distance from the contact for samples IG-2 and IG-3, but then decreased to 20.8 Ma for sample

TABLE 3B

Sample IR1 monazite compositions

Growth zone	*Primary*		*Secondary*	
n	11		11	
	Avg.	1σ	Avg.	1σ
P_2O_5	29.3	(1.4)	28.7	(1.4)
SiO_2	0.7	(1.6)	0.7	(0.3)
ThO_2	4.1	(0.8)	6.9	(2.2)
Y_2O_3	1.7	(0.6)	2.0	(0.6)
La_2O_3	13.5	(1.9)	11.1	(2.2)
Ce_2O_3	28.0	(2.2)	26.3	(2.1)
Pr_2O_3	2.8	(0.2)	2.9	(0.2)
Nd_2O_3	11.8	(0.7)	12.4	(0.9)
Sm_2O_3	2.1	(0.5)	2.8	(0.6)
Gd_2O_3	2.3	(0.4)	2.5	(0.2)
U_2O_3	0.2	(0.5)	0.2	(0.2)
CaO	1.1	(0.4)	1.1	(0.2)
Total	**97.8**		**97.6**	

TABLE 3C

Proterozoic gneiss monazite compositions and chemical ages

Sample	XG-2	XG-4	XG-5	XG-6	XG-7*	XG-9	XG-10	XG-11	XG-12
n	7	22	22	21	6	35	37	41	20
Avg. Age (Ma)	928	1246	1148	1274	N/A	1346	1385	1034	687
1 σ	390	360	451	397	N/A	332	118	366	657
P_2O_5	19.6	27.0	26.3	27.3	28.0	28.6	28.0	28.8	27.9
SiO_2	33.7	12.2	14.1	10.4	3.3	11.8	8.6	8.3	10.2
ThO_2	0.14	1.12	0.85	0.19	0.37	1.12	0.27	0.61	1.33
Y_2O_3	14.2	11.6	16.3	12.7	18.4	12.3	13.4	14.4	13.4
La_2O_3	22.3	25.6	27.1	28.5	33.9	26.2	29.4	29.4	27.5
Ce_2O_3	2.01	3.19	2.59	3.47	3.20	3.04	3.47	3.26	3.16
Pr_2O_3	6.11	13.1	8.51	13.6	9.96	12.1	13.4	12.2	11.9
Nd_2O_3	0.51	2.48	1.14	1.96	0.96	2.14	2.05	1.82	1.89
Sm_2O_3	0.22	1.69	0.72	0.91	0.42	1.38	1.05	1.03	1.32
Gd_2O_3	0.02	0.16	0.08	0.06	0.03	0.13	0.07	0.09	0.14
Tb_2O_3	0.04	0.51	0.28	0.11	0.11	0.42	0.15	0.25	0.44
Dy_2O_3	0.04	0.51	0.28	0.11	0.11	0.41	0.15	0.25	0.44
Er_2O_3	0.00	0.08	0.07	0.01	0.03	0.10	0.02	0.05	0.12
U_2O_3	0.34	0.42	1.38	0.16	0.01	0.63	0.19	0.26	0.36
PbO	0.95	0.61	0.45	0.47	0.00	0.64	0.43	0.33	0.27
Total	**100.3**	**100.3**	**100.2**	**100.0**	**98.9**	**101.0**	**100.7**	**101.0**	**100.3**

* Analysis of XG-7 yielded only two meaningful ages of 7 and 81 Ma.

IG-4 (fig. 8). Sample IG-5 farthest from the contact had an average monazite age lower than in samples IG-2 and IG-3. Thus, we see no systematic dependence of monazite alteration intensity on distance from the Searchlight contact.

We used a multi-collector IMP for *in-situ* measurements of oxygen isotope compositions of monazite grains from Ireteba granite samples collected near the Searchlight contact and dated by Townsend and others (2000). Figure 6 shows our measured $\delta^{18}O$ values and Th-Pb ages from Townsend and others (2000) for two representative monazite grains. Although patchy secondary zones yielded younger ages than primary magmatic zones (fig. 6C), aggregate $\delta^{18}O$ values showed no significant difference between primary and secondary zones (fig. 9). Unlike the Th-Pb ages reported for these samples, the distribution of $\delta^{18}O$ values for both primary and secondary zones is unimodal (table 5, fig. 9). Primary and secondary zones yielded mean $\delta^{18}O_{SMOW}$ values for IR1 of 7.8 permil (n = 9) versus 7.4 permil (n = 11), and for RMC3 of 8.3 permil (n = 7) versus 8.0 permil (n = 3). Applying a t-test showed that there was not a statistically significant difference between primary and secondary zones for IR1 (P = 0.14) or RMC3 (P = 0.55). Sample IR20 failed the Shapiro-Wilk normality test but gave median values of primary and secondary zones of 8.6 permil (n = 12) versus 9.2 permil (n = 3). Using a Mann-Whitney Rank Sum Test we found that there was not a statistically significant difference between primary and secondary zones (P = 0.61).

Proterozoic Gneiss

Proterozoic gneiss (XG) samples have silica ranging from 60 to 75 percent (table 1). Samples XG-2 and XG-7 are metaluminous, while all other samples are peraluminous. Samples are LREE-enriched, with concentrations ~200 x chondrite for LREE

ZTable 4

Ireteba granite monazite LA-ICP-MS age data

Sample	Grain #	spot #	$^{208}Pb/^{232}Th$ Age (ma)	1σ error	$^{207}Pb/^{206}Pb$ Age (Ma)	1 σ error	$^{206}Pb/^{238}U$ Age (Ma)	1 σ error	$^{207}Pb/^{235}U$ Age (Ma)	1 σ error
IG-1	1	10	17.3	0.5	3198	76	23.9	0.5	120	4
IG-1	1	11	17.9	0.5	2117	142	24	1	64	5
IG-1	1	12	18.9	0.7	4367	93	59.5	2.4	525	24
IG-2	21	6	50.3	1.5	2127	249	54	2	145	18
IG-2	19	7	48.6	1.4	3192	98	41.1	1.1	203	8
IG-2	15	8	30.7	1.1	817	313	17.5	0.6	24.9	9.6
IG-2	25	9	22.7	0.7	1981	298	23.5	1.3	60.5	9.7
IG-2	18	10	58.0	1.7	3514	155	91.1	4.0	481	30
IG-2	26	11	17.7	0.6	3590	59	35.3	0.7	223	5
IG-3	7	43	26.2	0.8	1332	280	24.3	0.8	42.1	9.0
IG-3	7	44	53.6	1.0	851	211	58.7	1.4	80.6	20.1
IG-3	7	45	50	1.0	2453	204	48.7	2.0	148	14
IG-3	6	50	57.7	1.2	2808	171	85	4	291	22
IG-3	6	51	50.1	1.2	2865	157	58.8	2.3	239	16
IG-3	6	52	61.1	1.3	4101	77	157	5	960	34
IG-3	5	53	53.5	1.1	509	199	57.7	1.1	68.9	27.0
IG-3	5	54	54.5	1.1	2564	181	69.9	3.2	222	19
IG-3	5	55	57.7	1.3	1877	250	62.1	2.2	139	19
IG-3	27	60	54.2	1.1	1138	438	53.5	2.4	86.4	33.5
IG-3	27	61	53.2	1.1	2191	221	46.1	1.9	130	14
IG-3	20	62	53.3	1.1	1941	276	64.3	2.8	141	21
IG-3	20	63	26.0	1.2	2655	185	25.2	1.1	95.6	7.9
IG-4	1	20	24.8	0.6	608	231	43.2	1.1	55.7	21.3
IG-4	1	21	27.2	0.7	1191	182	22.9	0.6	38.2	5.9
IG-4	1	22	19.9	0.7	911	186	31.9	0.8	47.6	9.8
IG-4	1	23	24.4	0.7	2139	273	24	1	64	9
IG-4	7	24	17.5	0.5	2774	172	21.3	0.9	80.5	6.1
IG-4	7	25	20.8	0.6	2205	328	27.2	1.6	80.8	12.9
IG-4	7	30	16.1	0.5	4135	78	32.2	1.0	279	10
IG-4	23	32	22.8	0.5	4180	93	39.0	1.4	338	15
IG-4	25	33	17.6	0.6	2142	205	20.5	0.9	56.8	5.9
IG-4	25	34	32.2	0.7	781	261	25.3	0.8	35.4	11.9
IG-4	10	35	17.0	0.7	3051	214	21.6	1.3	97	8.9
IG-4	10	40	17.7	0.5	2163	205	25.6	1.0	66.9	6.8
IG-4	10	41	17.3	0.5	3240	130	24.1	0.9	122	7
IG-4	21	42	19.4	0.7	2478	163	23.5	0.9	78.2	6.0
IG-5	26	14	49.1	1.6	2560	208	67.8	2.6	206	18
IG-5	10	15	15.3	0.5	2867	281	19.6	1.3	85.3	10.0
IG-5	1	16	15.4	0.7	476	142	17.4	0.2	21.2	6.3
IG-5	3	17	57.8	1.7	1808	243	60.5	1.9	136	19
IG-5	33	18	56.6	1.6	2452	258	73.7	3.7	229	27
IG-5	32	19	15.9	0.6	2947	256	25.5	1.8	113	13

and 5–50 x chondrite for HREE (fig. 10A). They display a high field strength element-depleted arc-like signature in Spider plots normalized to primitive mantle (fig. 10B; Crombie, ms, 2006).

Whole rock $\delta^{18}O$ values for the four samples of Proterozoic gneiss in the wall zone transect range from 8.3 to 12.4 permil (table 2), significantly different from $\delta^{18}O$

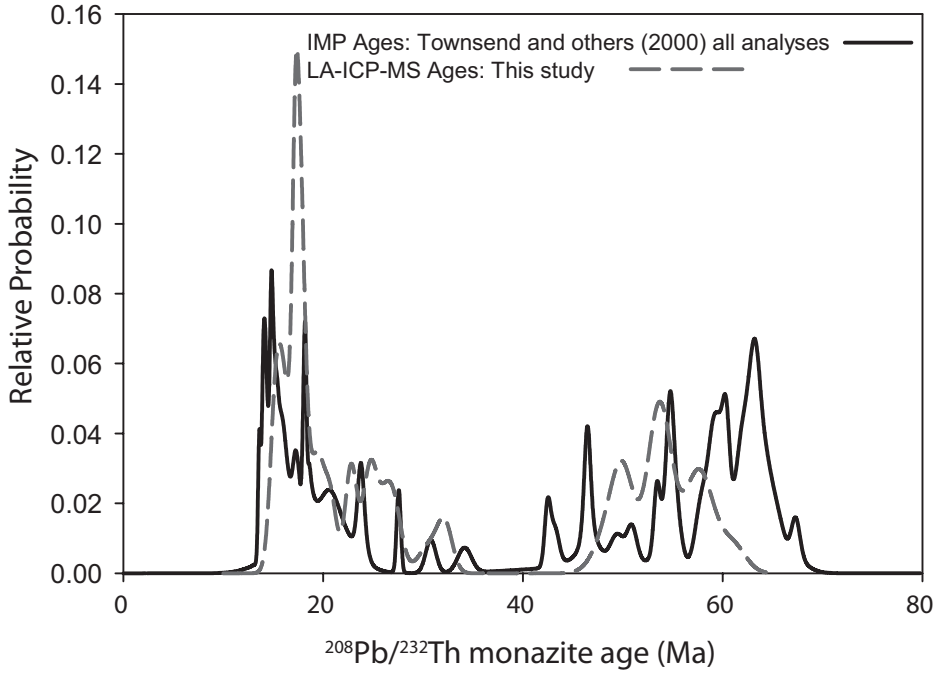

Fig. 7. Probability plot of Ireteba granite monazite $^{208}Pb/^{232}Th$ ages measured in this study and Townsend and others (2000) showing a bimodal age distribution. Measured ages fall between the ages of the Searchlight pluton (15.7 to 17.7 Ma) and the Ireteba pluton (66 Ma) because analyses overlapped age zones.

values previously obtained for middle and lower Searchlight rocks ($\delta^{18}O$ ~7.0‰; Bachl and others, 2001). Peraluminous gneisses with $\delta^{18}O > 10$ permil likely had an argillic sediment as their protolith and are therefore referred to as paragneisses. We found no systematic dependence of $\delta^{18}O$ values on distance from the contact (table 2, fig. 11), although the anomalously low $\delta^{18}O$ for the sample closest to the contact may reflect modification by the Searchlight pluton.

Results of EMP analyses of Proterozoic gneiss monazite grains are presented in table 3C, Appendix table A1 (ages) and Appendix table A2 (chemical compositions) (EMP images with numbered sample spot locations are available at http://earth.geology.yale.edu/~ajs/SupplementaryData/2013/02AyersEMP.pdf). Figure 12 shows BSE images of representative monazite grains from Proterozoic gneiss country rock. Monazite grains generally have (Th + U)/(Ca + Si) close to one, suggesting that the huttonite and brabantite substitutions are responsible for the incorporation of Th, U, Ca and Si. (Th + U) shows a 1:1 correlation with Si content but not Ca content, suggesting that huttonite exchange is the primary path for Th and U to enter monazite. As a result, concentrations of Th (fig. 12E) and Si (fig. 12F) show a strong positive correlation with BSE intensity (fig. 12D). Townsend and others (2000) showed the same trends in Ireteba monazite grains: secondary zones usually have higher Th and Si concentrations than primary zones.

We used both EMP and LA-ICP-MS dating methods to obtain ages of growth zones in monazite grains from Proterozoic gneiss samples. The samples collected from the wall zone (XG-4, XG-5, XG-6, XG-10, and XG-11) and the block in the lower Searchlight (XG-12) all yielded monazite. Monazite grains from these samples are mostly anhedral rounded grains 50 to 200 μm in diameter (fig. 12). BSE imaging of

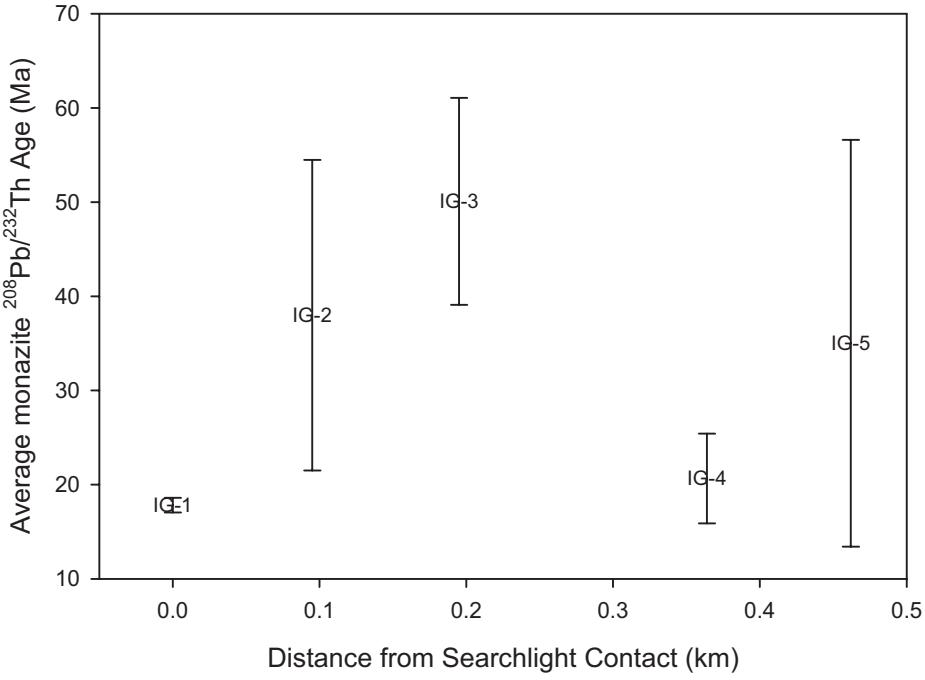

Fig. 8. $^{208}Pb/^{232}Th$ ages of monazite from Ireteba granite samples, all with one sigma error bars, plotted as a function of distance from the Searchlight contact. Error bars are large for samples IG-2, IG-3, and IG-5 because grains contained two age populations.

monazite grains from all six samples shows a variety of zoning within each sample. Wall zone samples contain abundant monazite grains with patchy zoning (figs. 12A, 12C, and 12D) and less common grains with a combination of patchy and concentric zoning (fig. 12B). The mixed-zone monazite grains typically have small concentrically zoned cores and thick rims with patchy zoning (fig. 12B). Some monazite zones display cross-cutting relationships suggesting veining along fractures. Sample XG-12 from the country rock block contained only patchy zoned monazite (figs. 12A and 12C). Relative BSE intensities of primary and secondary zones are not consistent from sample to sample; in sample XG-12 the younger secondary zones are darker than the older primary zones (figs. 12A and 12C) but in sample XG-6 the pattern is reversed (fig. 12B).

Samples from the roof zone contained almost no monazite. Sample XG-7, an orthogneiss from the roof zone, produced only one monazite grain during mineral separation. Four LA-ICP-MS analyses scattered all over the concordia diagram, but EMP analysis yielded ages of 7 and 81 Ma (Appendix table A1). We did not recover any monazite from samples XG-1, XG-3, XG-8, and XG-13, all augen orthogneisses from the roof zone. Sample XG-2, an augen orthogneiss, produced only one grain that yielded EMP ages of 412–1334 Ma (Appendix table A1).

In some samples measured ages correlate with zoning type. For example, in BSE images of monazite from sample XG-12 (figs. 12A and 12C) dark patches are secondary (EMP ages 14-45 Ma) and light patches are primary (EMP ages 1300-1500 Ma). In contrast, in monazite from sample XG-11 ages do not correlate with BSE intensity, although the youngest ages usually occur near edges of grains (fig. 12D).

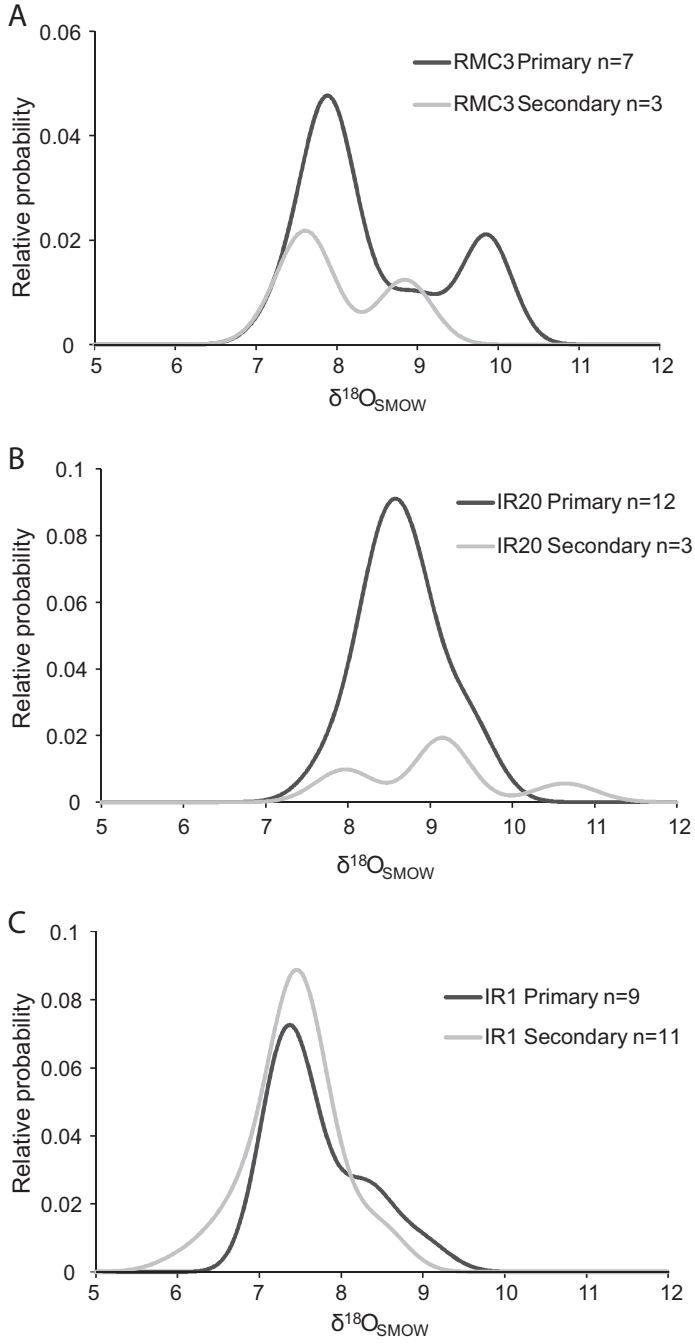

Fig. 9. Probability density plots of Ireteba granite monazite $\delta^{18}O_{SMOW}$ values of primary and secondary zones. (A) Sample RMC3. (B) Sample IR20. (C) Sample IR1.

A concordia plot of LA-ICP-MS monazite analyses from all wall zone samples and sample XG-12 defines a discordia line with intercepts of 1646 ± 9 Ma and 75 ± 61 Ma (table 6, fig. 13). Samples XG-11 and XG-12 have no concordant analyses. The Unmix

TABLE 5

Ireteba granite monazite oxygen isotope data

Sample	Primary $\delta^{18}O_{SMOW}$ (‰)	1σ*	Sample	Secondary $\delta^{18}O_{SMOW}$ (‰)	1σ*
IR1	7.60	0.45	IR1	7.59	0.51
IR1	8.99	0.47	IR1	6.15	0.50
IR1	8.22	0.48	IR1	7.52	0.46
IR1	7.26	0.44	IR1	7.02	0.46
IR1	7.37	0.51	IR1	6.65	0.47
IR1	8.36	0.45	IR1	7.33	0.46
IR1	7.41	0.46	IR1	7.59	0.46
IR1	7.59	0.50	IR1	7.43	0.44
IR1	7.34	0.46	IR1	8.49	0.46
IR20	8.29	0.50	IR1	7.87	0.46
IR20	9.42	0.46	IR1	7.51	0.48
IR20	8.35	0.47	IR20	10.65	0.51
IR20	8.01	0.51	IR20	7.97	0.49
IR20	8.57	0.47	IR20	9.16	0.46
IR20	7.80	0.47	RMC3	7.42	0.49
IR20	9.49	0.48	RMC3	8.85	0.47
IR20	8.39	0.44	RMC3	7.68	0.46
IR20	9.50	0.49			
IR20	8.79	0.44			
IR20	8.88	0.46			
IR20	8.54	0.51			
RMC3	8.98	0.47			
RMC3	9.87	0.45			
RMC3	7.93	0.46			
RMC3	7.86	0.44			
RMC3	8.15	0.49			
RMC3	7.41	0.47			
RMC3	8.13	0.49			

* Error estimated by summing error from analysis (small) and the spot-to-spot error determined by calculating the standard deviation over all analyses of standard 554 during the same analytical session.

routine and a probability density histogram of $^{207}Pb/^{206}Pb$ ages reveal a prominent peak at 1655 ± 2 Ma (1 σ, 83% of analyses) corresponding to the timing of intrusion of felsic magmas in the eastern Mojave between 1.62 and 1.69 Ga and to a metamorphic event recorded nearby by monazite at ~1.67 Ga (Wooden and Miller, 1990; Strickland and others, 2013; fig. 14). A probability density histogram of $^{208}Pb/^{232}Th$ ages also yields a peak at 1655 Ma (not shown). The Unmix routine in Isoplot yields a second, small age population of 1558 ± 6 Ma (1 σ, 17% of analyses).

Appendix table A1 contains BSE images of grains analyzed using the RPI Cameca SX-100 EMP. Analysis spot numbers are keyed to a table with measured chemical ages, one sigma analytical errors, and age errors estimated using Monte Carlo analysis. Figure 12 shows EMP analysis spot locations and ages for select Proterozoic gneiss monazite grains. The EMP age distribution (fig. 15) is different from the LA-ICP-MS $^{207}Pb/^{206}Pb$ age distribution (fig. 14). The main age peak is at 1412 Ma and the age distribution skews toward younger ages. A peak at 65 Ma corresponds to the age of the underlying Ireteba granite. Monazite grains from all samples that overlie the Ireteba pluton (fig. 3) show age evidence of intrusion of the Ireteba granite. Ages between ~40 to 80 Ma yield a distinct age population with mean = 63.8 ± 4.8 Ma (95% confidence

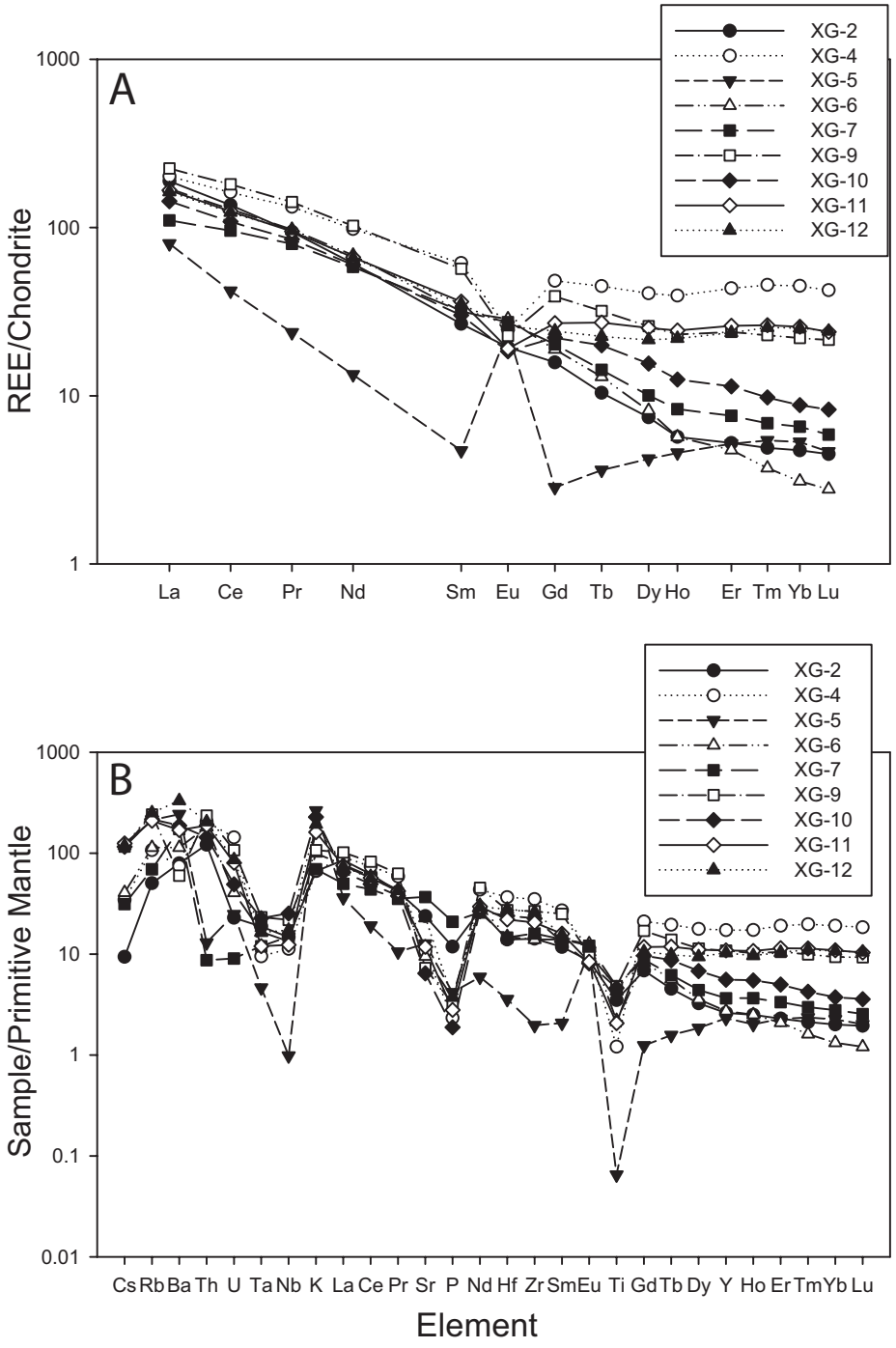

Fig. 10. Proterozoic gneiss whole rock trace element compositions. (A) Chondrite normalized REE diagram. Chondrite values from Boynton (1984). (B) Concentrations normalized to primitive mantle (Sun and McDonough, 1989).

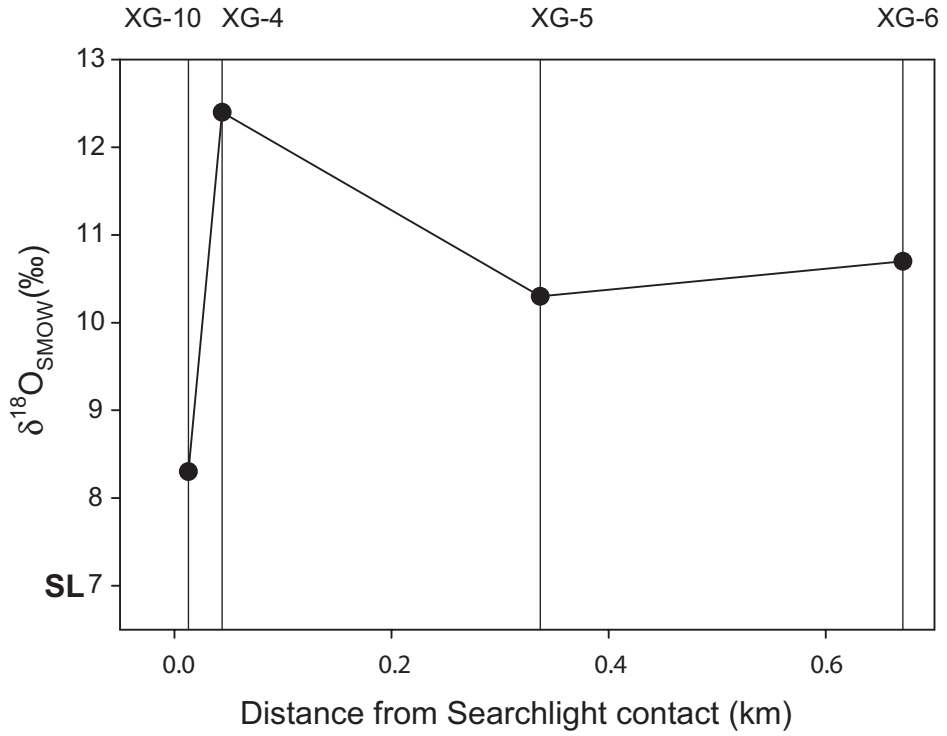

Fig. 11. Proterozoic gneiss whole rock oxygen isotope compositions. $\delta^{18}O_{SMOW}$ plotted as a function of distance from the Searchlight contact. "SL" indicates the average $\delta^{18}O_{SMOW}$ of two Searchlight pluton samples (Bachl and others, 2001).

limits), n = 13, and MSWD = 6.9 (Appendix table A1), so we conclude that a monazite growth or recrystallization event occurred at ~65 Ma. No corresponding concordant ages were found using LA-ICP-MS due to the very small size of the ~65 Ma age domains (fig. 12), but the lower intercept age of 75 ± 61 Ma from the LA-ICP-MS concordia diagram (fig. 13) likely corresponds to this event. Only one analysis out of 208 analyses yields an age within 1σ of the Searchlight pluton crystallization age, so we conclude that Searchlight intrusion and Miocene deformation did not cause the patchy zoning in Proterozoic gneiss monazite grains.

The oldest EMP ages (<1500 Ma, fig. 15) are much younger than LA-ICP-MS $^{207}Pb/^{206}Pb$ ages that peak at 1655 Ma (fig. 14). This discrepancy cannot be due to Pb loss, because some LA-ICP-MS analyses yield concordant ~1650 Ma ages (fig. 13), and must be the result of a systematic error. We are confident that the LA-ICP-MS ages are more accurate than the EMP ages because we used two different isotopic systems (U-Pb and Th-Pb) and different standards and obtained similar results. Furthermore, our LA-ICP-MS analyses reproduced the ages of secondary standards and of samples previously dated using IMP (see Methods section).

Zircon grains from Proterozoic gneiss samples show concentric oscillatory and sector zoning interpreted as magmatic (fig. 16). Zircon U-Pb ages were measured using LA-ICP-MS on samples XG-2, XG-5, XG-6, XG-7, XG-8, XG-11, XG-12, and XG-13 (table 7). Zircon was not recovered from samples XG-10 and XG-4. Technical problems led us to throw out the data for sample XG-1. A probability plot of zircon $^{207}Pb/^{206}Pb$ ages pooled from the eight samples shows peaks at 1720 and 1035 Ma (fig.

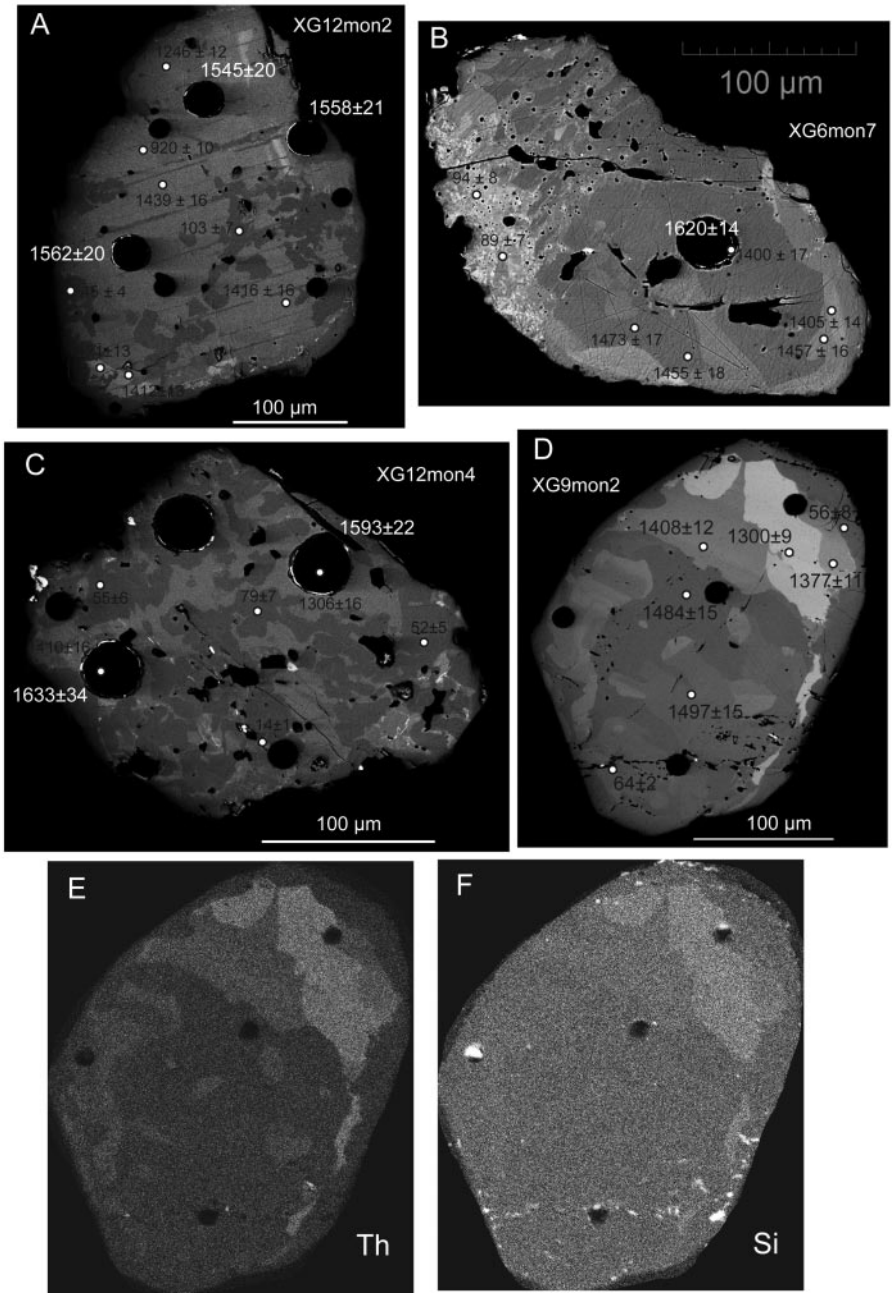

Fig. 12. Backscattered electron images of Proterozoic gneiss monazite showing patchy and chaotic internal zoning. LA-ICP-MS analysis pits labeled white with $^{207}Pb/^{206}Pb$ ages in Ma and 1σ errors. EMP analysis spots labeled black with ages in Ma and 1σ errors. (A) XG12mon2. (B) XG6mon7. (C) XG12mon4. (D) XG9mon2. (E) Th x-ray map of XG9mon2. (F) Si x-ray map of XG9mon2.

Table 6

Proterozoic gneiss monazite LA-ICP-MS age data

Analysis	Sample	$^{208}Pb/^{232}Th$ (Ma)	1σ error	$^{207}Pb/^{206}Pb$ (Ma)	1σ error	$^{206}Pb/^{238}U$ (Ma)	1σ error	$^{207}Pb/^{235}U$ (Ma)	1σ error
83_XG10mon6	XG-10	1679	45	1659	16	1815	18	1742	24
84_XG10mon6	XG-10	1601	43	1638	46	1918	26	1786	55
85_XG10mon3	XG-10	1623	43	1672	27	1756	19	1717	33
86_XG10mon3	XG-10	1613	43	1676	27	1762	20	1722	33
87_XG10mon8	XG-10	1096	30	1636	24	1414	15	1504	27
88_XG10mon27	XG-10	1668	44	1680	15	1577	16	1620	22
89_XG10mon31	XG-10	1618	43	1581	44	1911	23	1757	53
990_XG10mon31	XG-10	1644	44	1668	41	1921	22	1802	49
991_XG10mon30	XG-10	1667	44	1613	17	1878	18	1755	25
992_XG10mon14	XG-10	1444	39	1637	24	1666	17	1653	30
993_XG10mon15	XG-10	1524	41	1638	21	1794	18	1723	28
994_XG10mon19	XG-10	1632	43	1608	28	1897	20	1763	35
09_XG10mon11	XG-10	1505	39	1628	23	1611	16	1624	28
10_XG10mon11	XG-10	1529	39	1572	23	1649	16	1620	29
11_XG10mon29	XG-10	1557	40	1665	28	1681	17	1678	33
12_XG10mon2	XG-10	1555	40	1634	30	1759	18	1706	36
13_XG10mon1	XG-10	1517	39	1654	29	1613	17	1633	33
14_XG10mon26	XG-10	1361	35	1661	12	1601	15	1628	19
15_XG10mon26	XG-10	1486	38	1620	18	1544	15	1577	23
16_XG10mon24	XG-10	1530	39	1721	42	1562	18	1631	44
24_XG11mon1	XG-11	1232	32	1633	27	1408	15	1493	29
25_XG11mon2	XG-11	1215	31	1578	25	1269	13	1381	26
26_XG11mon3	XG-11	874	23	1598	20	1104	11	1275	20
27_XG11mon4	XG-11	1220	31	1558	14	1342	13	1418	19
28_XG11mon4	XG-11	1200	31	1583	15	1361	13	1440	19
29_XG11mon4	XG-11	786	21	1474	18	1077	11	1206	19
41_XG12mon1	XG-12	928	24	1679	20	901	9	1139	18
Sept180735	XG-12	679	4	1560	22	673	5	916	6
Sept180736	XG-12	436	3	1547	30	378	3	596	6
Sept180737	XG-12	549	4	1537	25	587	4	826	6
Sept180738	XG-12	1031	7	1593	22	1043	7	1236	7
Sept180740	XG-12	580	4	1633	34	629	5	898	10
Sept180741	XG-12	1089	7	1562	20	1108	8	1272	6
Sept180742	XG-12	888	6	1558	21	990	7	1184	7
Sept180743	XG-12	1023	7	1545	20	1090	8	1253	6
Sept180744	XG-12	598	4	1655	28	613	5	888	8
10_XG-4mon1	XG-4			1666	7	1802	3	1740	8
11_XG-4mon1a	XG-4			1655	9	2482	5	2057	12
13_XG-4mon6a	XG-4			1653	10	1637	3	1644	11
15_XG-4mon10a	XG-4			1705	13	1520	4	1600	13
27_XG-4mon2	XG-4			1687	13	1582	4	1628	13
28_XG-4mon2a	XG-4			1664	9	1697	3	1683	10
29_XG-4mon19	XG-4			1655	8	1764	3	1715	9
30_XG-4mon19a	XG-4			1645	9	1776	3	1717	10
40_XG4mon3	XG-4			1621	12	1613	4	1617	13

TABLE 6
(continued)

Analysis	Sample	$^{208}Pb/^{232}Th$ (Ma)	1σ error	$^{207}Pb/^{206}Pb$ (Ma)	1σ error	$^{206}Pb/^{238}U$ (Ma)	1σ error	$^{207}Pb/^{235}U$ (Ma)	1σ error
83_XG10mon6	XG-10	1679	45	1659	16	1815	18	1742	24
41_XG4mon3a	XG-4			1612	11	1640	4	1628	11
42_XG4mon3b	XG-4			1682	16	1551	5	1608	16
43_XG4mon5	XG-4			1643	11	1855	4	1758	13
45_XG4mon9	XG-4			1622	15	1619	5	1621	15
58_XG-5mon1	XG-5			1796	79	985	15	1272	59
59_XG-5mon2	XG-5			1630	16	1684	5	1660	17
60_XG-5mon2a	XG-5			1653	28	1939	10	1805	32
61_XG-5mon10	XG-5			1696	44	1533	12	1603	43
09_XG5mon11	XG-5	1647	44	1677	15	1659	16	1666	22
10_XG5mon11	XG-5	1638	43	1667	22	1749	18	1712	29
11_XG5mon12	XG-5	1438	38	1651	20	1603	16	1624	25
12_XG5mon12	XG-5	1449	39	1680	18	1682	16	1680	24
24_XG5mon4	XG-5	1540	41	1698	19	1705	17	1701	25
25_XG5mon5	XG-5	1664	44	1661	12	1686	16	1674	20
26_XG5mon5	XG-5	1511	40	1650	51	2166	31	1913	66
27_XG5mon19	XG-5	1645	44	1666	13	1648	16	1655	20
28_XG5mon19	XG-5	1621	43	1638	17	1601	16	1616	23
29_XG5mon6	XG-5	1612	43	1687	26	1742	18	1716	32
39_XG5mon6	XG-5	1393	37	1658	14	1766	17	1716	22
40_XG6mon10	XG-6	1623	43	1661	16	1627	16	1641	22
41_XG6mon10	XG-6	1638	44	1690	30	1550	18	1609	34
43_XG6mon23	XG-6	65	2	1647	31	1905	21	1784	39
53_XG6mon19	XG-6	798	22	1693	18	1451	15	1551	23
54_XG6mon6	XG-6	1676	45	1637	19	1821	18	1736	27
55_XG6mon6	XG-6	1475	39	1694	31	1539	18	1605	35
56_XG6mon6	XG-6	1185	32	1680	34	1540	18	1599	37
57_XG6mon4	XG-6	1470	39	1652	27	1638	18	1643	32
58_XG6mon4	XG-6	1450	39	1643	16	1665	16	1654	23
68_XG6mon7	XG-6	1551	41	1620	14	1753	17	1692	22
69_XG6mon1	XG-6	1573	42	1684	17	1602	16	1636	23
70_XG6mon9	XG-6	1471	39	1657	24	1683	18	1670	30
71_XG6mon9	XG-6	1431	38	1661	18	1580	16	1614	24

14). The older age corresponds to the Ivanpah orogeny of the Mojave province (Wooden and Miller, 1990), but the significance of the 1035 Ma age is unknown.

DISCUSSION

Intrusion of the Searchlight pluton at 16 to 17 Ma led to the formation of the extensive hydrothermal ore deposits of gold and silver that make up the historic Searchlight mining district (Callaghan, 1939). The deposits are in the roof zone immediately above the upper Searchlight unit, hosted by hydrothermally altered Miocene volcanics and Precambrian gneisses that contain abundant thick quartz veins.

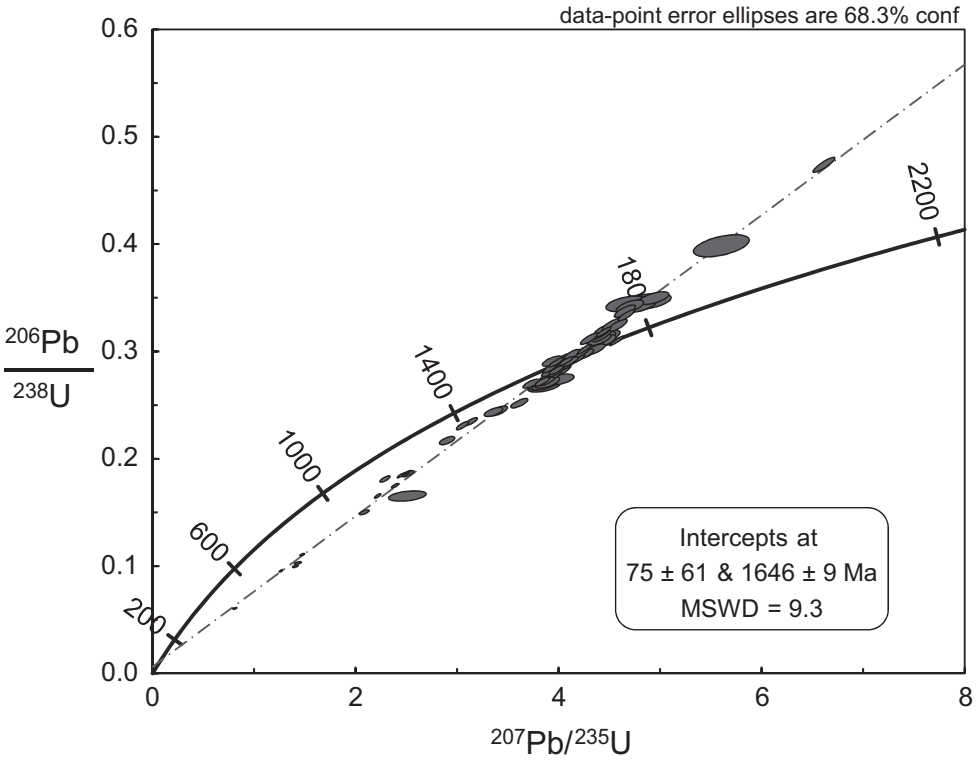

Fig. 13. Concordia diagram for monazite from all Proterozoic wall zone samples and XG-12.

These features suggest that the Searchlight pluton released abundant magmatic fluid (Faulds and others, 2002; Ludington and others, 2005; Lledo and Cline, 2008). The pluton may also have heated overlying groundwaters and accelerated groundwater circulation. Thus, we expected that whole rocks, monazite grains and perhaps even zircon grains in shallow country rocks near the roof zone would provide abundant evidence of hydrothermal alteration.

The two primary mechanisms for fluids to infiltrate country rock are porous flow, and hydrofracturing leading to dike or vein formation. In this study we attempted to evaluate the broader effects of porous flow rather than localized effects due to dike and vein flow by collecting samples far removed from veins. The pervasive alteration and the disseminated nature of the ore metals in the roof zone are consistent with porous flow, but abundant veins suggest that hydrofracturing also occurred, implying brittle behaviour. Quartz veins (as large as 1 m thick) are prominent along the contact of the middle Searchlight unit and the Proterozoic wall zone rocks, and are most abundant in the roof zone. Quartz veins are smaller and less common along the Searchlight-Ireteba contact. We avoided these veins during sample collection to reduce the possibility of localized fluid effects on monazite grains. However, we collected sample XG-10 close to the contact, so the proximity of quartz veins to this sample was unavoidable.

Ireteba Granite

Ireteba granite samples show little evidence of hydrothermal alteration other than minor sericitization of plagioclase and chlorite replacement of biotite. Deeper levels of the pluton display a strong ductile deformational fabric.

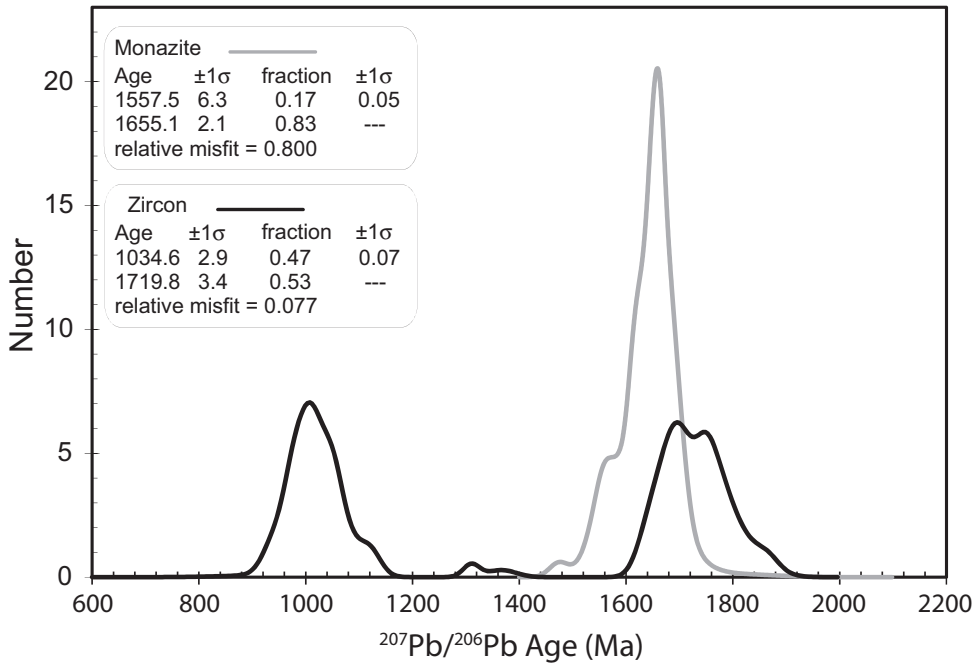

Fig. 14. Probability density plot of zircon $^{207}Pb/^{206}Pb$ ages for all Proterozoic gneiss samples except XG-1 and monazite $^{207}Pb/^{206}Pb$ ages for wall zone Proterozoic gneiss samples and XG-12. Text boxes contain ages obtained by deconvolving the age spectra using the Isoplot Unmix routine (Ludwig, 2000).

Figure 6A shows that primary domains with magmatic zoning and Ireteba crystallization ages are overprinted by secondary domains with patchy zoning and ages close to Searchlight crystallization ages. Monazite grains from all Ireteba granite samples (IG-1, IG-2, IG-3, IG-4, and IG-5) yield ages similar to the crystallization age of the ~16 to 17 Ma Searchlight pluton. Pooled monazite ^{232}Th-^{208}Pb ages display a bimodal age distribution with peaks at ~19 Ma (similar to the 16.5 Ma Searchlight age) and ~54 Ma (fig. 7).

Although Ireteba monazite grains show two distinct age populations (fig. 7), we observed only one population of $\delta^{18}O$ values in each sample (fig. 9, table 5). We believe the ~15 to 20 μm IMP spot size gave us sufficient spatial resolution to obtain clean analyses of primary and secondary zones (fig. 6). The spatial resolution of our IMP $\delta^{18}O$ analyses was better than for our LA-ICP-MS age measurements, which was good enough to distinguish two age populations. If there are multiple $\delta^{18}O$ populations, their differences are smaller than can be detected given the 1σ precision of ±0.1 permil of our measurements.

If infiltrating fluid had induced monazite dissolution-reprecipitation, we would expect a shift in oxygen isotope composition of secondary zones resulting from oxygen isotope exchange with the fluid phase. That primary and secondary zones in monazite grains show no significant difference in $\delta^{18}O$ composition suggests that fluids did not cause the formation of secondary zones within Ireteba monazite grains, an interpretation consistent with whole rock oxygen isotope compositions of samples collected along the transect into the Ireteba granite, which show no systematic changes in $\delta^{18}O$ values with distance from the Searchlight contact (fig. 5).

An alternative explanation of secondary zone formation is that the fluid/rock ratio at the time of alteration was low so that the rock buffered the composition of the

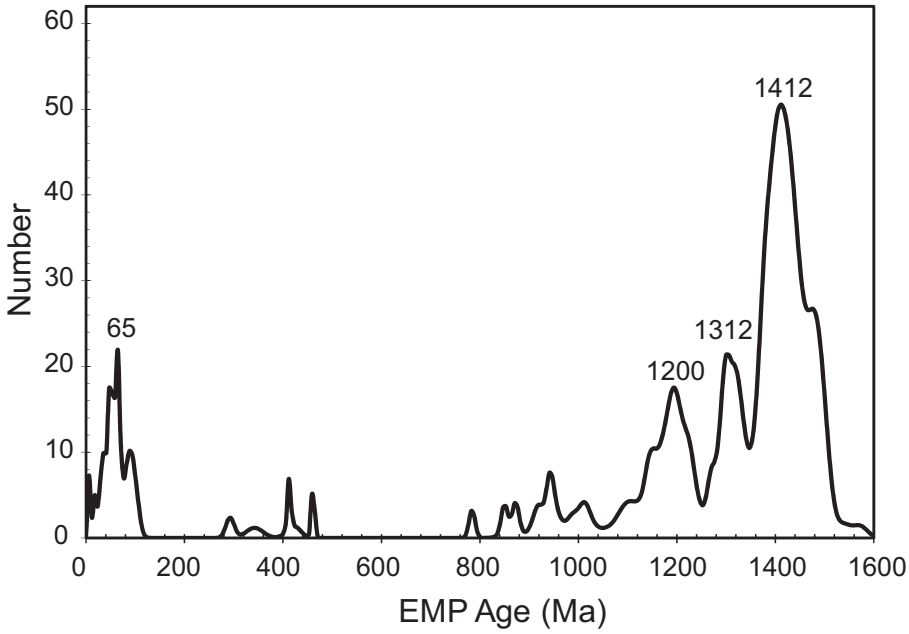

Fig. 15. Probability density plot of Proterozoic gneiss monazite chemical ages measured using EMP.

fluid. In this case, infiltrating fluid would have been close to isotopic equilibrium with monazite grains, and oxygen isotope exchange during dissolution-precipitation would not cause a significant shift in $\delta^{18}O$. Magmatic fluids released from the Searchlight pluton would have had $\delta^{18}O$ values similar to that of the Searchlight pluton at ~7.0 permil (isotopic fractionation at such high temperatures would result in small differences). If small volumes of fluid entered the Ireteba granite, they would quickly acquire its $\delta^{18}O$ of ~8.5 to 9 permil and be close to equilibrium with primary monazite grains that have $\delta^{18}O$ of 7.8 permil. The secondary zones in IR-1 monazite grains have an average $\delta^{18}O$ of 7.4 permil, intermediate between Searchlight and Ireteba whole rock values and close to Ireteba monazite primary values. This suggests that the Ireteba granite could have buffered the $\delta^{18}O$ of the infiltrating fluids, masking the signature of the fluid source, the Searchlight pluton. However, this would not explain the variable whole rock oxygen isotope compositions (8.1‰ to 9.5‰) that show no correlation with distance to the contact.

Because country rocks contain much less exchangeable hydrogen than oxygen, fluids must travel greater distances to reach hydrogen isotopic equilibrium with unaltered host rock. Searchlight magmatic fluids would impose their hydrogen isotope composition on country rocks near the contact. Thus, hydrogen isotopes should be an even more sensitive indicator of alteration by externally-derived fluids than oxygen isotopes. Although whole rock hydrogen isotope compositions of Ireteba transect samples show variation in δD (−87‰ to −98‰), they do not show a distinct pattern related to the Searchlight pluton (fig. 5), further supporting the interpretation that the Searchlight pluton released little fluid into the northern margin wall rocks. Finally, average monazite $^{208}Pb/^{232}Th$ ages of samples collected along the Ireteba granite transect show no systematic dependence on distance from the contact (fig. 8).

None of our chemical and isotopic proxies for intensity of hydrothermal alteration show a systematic spatial relationship to the Searchlight pluton. This suggests that

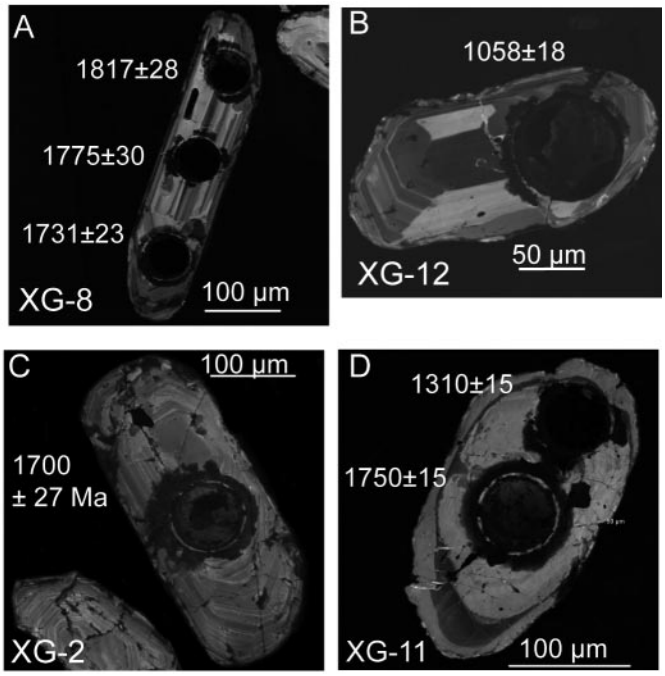

Fig. 16. CL images of Proterozoic gneiss zircon grains with laser ablation pits labelled with $^{207}Pb/^{206}Pb$ ages in Ma and one sigma errors. (A) XG-8. (B) XG-12. (C) XG-2. (D) XG-11.

Searchlight-derived magmatic fluids did not alter Ireteba monazite grains and induce the formation of the secondary zones. Hydrothermal alteration by meteoric water also seems unlikely, since whole rocks and monazite in the wallrock do not show the expected shift to isotopically lighter values. However, the fact remains that secondary zones formed within Ireteba granite monazite grains at approximately the time of the Searchlight intrusion.

In previous studies of the Ireteba granite Townsend and others (2000) and Loflin (ms, 2002) reported that the intensity of monazite alteration (proportion of secondary monazite) at the time of the Searchlight intrusion increased with decreasing distance from the Searchlight contact and increasing paleodepth. However, in this study we found that intensity of monazite alteration in the Ireteba granite does not correlate with distance from the contact (fig. 8), which is inconsistent with alteration induced by magmatic fluids (mechanisms 3 and 5-7 in fig. 1) or magmatic heat (mechanisms 2 or 8).

The most altered monazite grains in the studies of Townsend and others (2000) and Loflin (ms, 2002) came from the greatest paleodepth, approximately the same paleodepth as the Ireteba granite samples in this study. At the time of the Searchlight intrusion those samples were at the greatest depths and highest temperatures, facilitating ductile deformation. Tectonic deformation during and after intrusion of the Searchlight pluton led to the development of a mylonite zone in the lowermost Searchlight and the deepest portions of the Ireteba granite. Monazite grains in Ireteba samples that were at the greatest paleodepths (samples RMC3 and IR1, compare fig. 3) partially recrystallized to form patchy secondary zones with Miocene ages (mechanism 9 in fig. 1, fig. 6C). In contrast, abundant veins suggest that shallower Proterozoic gneiss samples behaved rigidly, and their monazite grains lack Miocene ages. This

Table 7

Proterozoic gneiss zircon LA-ICP-MS age data

Analysis	Sample	$^{207}Pb/^{206}Pb$ (Ma)	1σ error	$^{206}Pb/^{238}U$ (Ma)	1σ error	$^{207}Pb/^{235}U$ (Ma)	1σ error	Th/U
Sept170724	XG-1	1543	15	156	1	284	1	0.81
Sept170723	XG-1	1467	16	170	1	296	1	1.83
Sept170722	XG-1	1361	17	218	1	351	2	0.85
Sept170721	XG-1	996	16	238	1	323	1	0.57
Sept170720	XG-1	1284	16	148	1	241	1	0.25
Sept170719	XG-1	1731	14	221	1	418	1	
Sept170714	XG-1	2446	18	788	9	1369	9	0.45
Sept170713	XG-1	2088	18	420	5	801	7	2.38
Sept170712	XG-1	1764	23	1081	12	1334	10	0.47
Sept170711	XG-1	2155	18	669	8	1124	8	1.92
Sept170709	XG-1	1935	19	602	7	970	8	0.66
Sept170708	XG-1	1912	19	636	7	998	8	0.54
Sept170707	XG-1	1712	19	1275	14	1448	9	0.54
Sept170706	XG-1	1760	24	462	5	754	8	0.18
Sept170705	XG-1	1703	20	623	7	914	7	0.36
Jul050759	XG-1	2179	17	739	9	1201	8	0.63
Jul050758	XG-1	1908	17	881	10	1225	9	0.41
Jul050757	XG-1	2174	17	627	7	1081	8	0.83
Jul050756	XG-1	2162	17	538	6	973	8	0.62
Jul050755	XG-1	2349	17	471	6	954	7	0.79
Jul050754	XG-1	2136	18	732	9	1177	8	0.84
Jul050753	XG-1	1977	18	733	9	1116	8	1.35
Jul050752	XG-1	1930	17	1367	15	1598	10	0.87
Jul050751	XG-1	2343	17	880	10	1408	9	1.28
Sept170725	XG-1	1818	14	147	1	307	1	1.21
Sept170710	XG-1	1947	19	747	8	1123	8	1.65
Jul050760	XG-1	2689	16	379	5	940	7	0.72
Jul050744	XG-2	1796	27	1615	18	1695	13	0.44
Jul050742	XG-2	1750	30	1647	19	1693	14	0.50
Jul050741	XG-2	1710	26	1633	18	1667	13	0.45
Jul050740	XG-2	1751	25	1705	19	1726	13	0.51
Jul050739	XG-2	1741	31	1702	20	1720	15	0.67
Jul050738	XG-2	1716	26	1692	19	1704	13	0.37
Jul050737	XG-2	1749	26	1707	19	1726	13	0.53
Jul050736	XG-2	1713	41	1648	21	1677	19	0.48
Jul050735	XG-2	1700	27	1648	19	1671	13	0.33
Jul050734	XG-2	1776	25	1772	20	1775	13	0.51
Jul050733	XG-2	1714	28	1744	20	1731	14	0.54
Jul050732	XG-2	1701	25	1792	20	1751	13	0.49
Jul0607B112	XG-5	1824	42	1674	21	1746	20	
Jul0607B113	XG-5	1750	37	1617	19	1680	17	
Jul0607B114	XG-5	1793	31	1566	17	1669	15	
Jul0607B115	XG-5	1684	158	1513	46	1590	71	
Jul0607B116	XG-5	1747	23	1639	17	1691	12	
Jul0607B117	XG-5	1777	36	1650	19	1711	17	

TABLE 7
(continued)

Analysis	Sample	$^{207}Pb/^{206}Pb$ (Ma)	1σ error	$^{206}Pb/^{238}U$ (Ma)	1σ error	$^{207}Pb/^{235}U$ (Ma)	1σ error	Th/U
Jul0607B118	XG-5	1782	24	1673	17	1726	12	
Jul0607B119	XG-5	1765	26	1665	18	1714	13	
Jul0607B120	XG-5	1853	33	1342	15	1557	15	
Jul0607B121	XG-5	1768	38	1497	18	1617	18	
Jul0607B122	XG-5	2037	35	2382	27	2206	18	
Sept170740	XG-6	985	17	545	2	639	2	0.24
Sept170739	XG-6	1014	32	467	3	572	6	0.14
Sept170738	XG-6	951	88	468	7	559	18	0.12
Sept170737	XG-6	1014	21	506	2	609	4	0.11
Sept170736	XG-6	1080	17	549	2	665	3	0.20
Sept170735	XG-6	1038	17	521	2	629	3	0.52
Sept170734	XG-6	982	22	486	2	584	4	0.15
Sept170733	XG-6	1061	16	533	2	646	2	0.10
Sept170728	XG-6	1026	25	538	3	642	5	0.36
Sept170727	XG-6	993	21	544	2	640	4	0.28
Sept170726	XG-6	1122	18	545	2	672	3	0.15
Jul0607B67	XG-7	1107	23	444	2	569	4	0.54
Jul0607B66	XG-7	966	33	379	2	474	6	0.59
Jul0607B65	XG-7	1034	27	448	2	558	5	0.38
Jul0607B64	XG-7	1047	29	462	3	574	6	0.62
Jul0607B63	XG-7	995	21	468	2	569	4	0.49
Jul0607B62	XG-7	1019	21	469	2	575	4	0.54
Jul0607B61	XG-7	1016	37	401	3	506	7	0.49
Jul0607B60	XG-7	1053	20	450	2	563	3	0.50
Jul0607B59	XG-7	1046	20	475	2	586	3	0.60
Jul0607B088	XG-8	1837	43	1368	18	1562	19	
Jul0607B087	XG-8	1750	29	1393	16	1540	13	
Jul0607B086	XG-8	1817	28	1680	19	1741	14	
Jul0607B085	XG-8	1775	30	1513	18	1625	14	
Jul0607B084	XG-8	1731	23	1515	17	1607	12	
Jul0607B083	XG-8	1698	27	1666	19	1679	13	
Jul0607B082	XG-8	1762	27	1796	20	1780	14	
Jul0607B081	XG-8	1815	32	1469	18	1616	15	
Jul0607B080	XG-8	1745	22	1706	19	1723	12	
Jul0607B079	XG-8	995	22	462	2	561	4	
Jul0607B078	XG-8	995	19	463	2	562	3	
Jul0607B077	XG-8	1026	24	484	2	590	5	
Jul0607B076	XG-8	989	30	479	3	577	6	
Jul0607B075	XG-8	1367	27	377	2	553	5	
Jul0607B074	XG-8	1124	22	436	2	564	4	
Sept180714	XG-11	1044	19	524	2	632	3	0.21
Sept180713	XG-11	951	24	503	2	592	5	0.09
Sept180712	XG-11	1017	24	434	2	539	4	0.41
Sept180711	XG-11	935	21	448	2	536	3	0.05
Sept180710	XG-11	965	18	394	2	489	2	0.18

Table 7
(continued)

Analysis	Sample	$^{207}Pb/^{206}Pb$ (Ma)	1σ error	$^{206}Pb/^{238}U$ (Ma)	1σ error	$^{207}Pb/^{235}U$ (Ma)	1σ error	Th/U
Sept180709	XG-11	1013	15	493	2	595	2	0.03
Sept180708	XG-11	1009	16	545	2	643	2	0.03
Sept180707	XG-11	976	16	484	2	579	2	0.02
Sept180706	XG-11	971	18	462	2	558	3	0.10
Sept180705	XG-11	937	18	385	1	475	2	0.05
Sept170743	XG-11	996	20	463	2	565	3	0.20
Sept170742	XG-11	1310	15	568	2	743	2	0.11
Sept170741	XG-11	1750	15	742	3	1047	4	0.43
Jul0607B34	XG-11	1007	20	410	2	514	3	0.22
Jul0607B47	XG-12	1660	25	1786	20	1728	13	0.63
Jul0607B46	XG-12	1701	28	1680	19	1689	14	0.50
Jul0607B45	XG-12	1707	31	1713	20	1710	15	0.32
Jul0607B44	XG-12	1692	25	1453	17	1553	12	0.48
Jul0607B43	XG-12	1676	25	1744	19	1713	12	0.64
Jul0607B42	XG-12	1701	26	1742	20	1723	13	0.51
Jul0607B41	XG-12	1058	18	492	2	605	3	0.46
Jul0607B40	XG-12	967	19	452	2	548	3	0.20
Jul0607B39	XG-12	1027	16	500	2	606	2	0.71
Jul0607B38	XG-12	1005	18	463	2	566	3	0.41
Jul0607B37	XG-12	1050	16	489	2	601	2	0.48
Jul0607B36	XG-12	1093	20	436	2	558	3	0.61
Jul0607B35	XG-12	1053	21	495	2	608	4	0.47
Jul050781	XG-13	1689	20	1172	12	1359	9	0.31
Jul050779	XG-13	1665	20	1230	12	1390	9	0.25
Jul050778	XG-13	1638	20	1055	11	1256	8	0.35
Jul050776	XG-13	1670	21	1486	15	1556	10	0.34
Jul050775	XG-13	1647	21	1638	17	1634	10	0.41
Jul050774	XG-13	1677	21	1266	13	1420	9	0.26
Jul050773	XG-13	1697	22	1508	16	1581	10	0.35
Jul050772	XG-13	1866	20	1353	14	1559	10	0.19
Jul050771	XG-13	1683	21	1559	16	1606	10	0.39
Jul050770	XG-13	1659	20	1415	15	1509	10	0.40
Jul050769	XG-13	1765	22	1585	17	1657	11	0.42
Jul050768	XG-13	1629	20	1470	16	1530	10	0.16
Jul050767	XG-13	1647	20	1333	15	1453	9	0.21
Jul050766	XG-13	1701	20	1347	15	1485	10	0.24
Jul050765	XG-13	1694	21	1651	18	1665	11	0.33

interpretation is consistent with the observations of Townsend and others (2000), who state "Deeper levels of the Ireteba and Miocene plutons were ductilely deformed at 15–16 Ma. At shallow levels remote from the Miocene plutons, the Ireteba granite appears to have experienced little Miocene heating and deformation . . . Irregularly shaped patchy zones with high huttonite component ($ThSiO_4$) are widespread in

monazite at deep levels adjacent to Miocene plutons but less common in shallow-level rock; monazite grains with extensive replacement generally have irregular, embayed surfaces. In undeformed rocks distant from the Miocene plutons, monazites are less modified and more nearly euhedral, though fine networks of replacement veins are common and irregular rims are evident in some grains." Our additional observations lead us to conclude that only rocks in the Searchlight roof zone were hydrothermally altered and contain metal ores, suggesting that hydrothermal fluids were tightly focused in the roof zone above the brittle- to ductile transition.

Proterozoic Gneiss

Samples collected along the transect perpendicular to the Searchlight contact and extending into the Proterozoic gneisses show no correlation between distance and whole rock oxygen isotope composition (fig. 11). There is significant variability in whole rock $\delta^{18}O$ values in the Proterozoic gneiss wall zone distal to the contact that is probably inherited from the protolith (10.3‰ to 12.4‰, table 2), but sample XG-10 at the contact has a whole rock $\delta^{18}O$ of 8.3 permil that is closer to $\delta^{18}O$ values previously obtained for middle and lower Searchlight rocks ($\delta^{18}O$ ~7.0‰; Bachl and others, 2001), which may reflect oxygen isotope exchange associated with intrusion of the Searchlight.

The rarity of monazite grains in roof zone samples suggests either an initial dearth of monazite grains or destruction of pre-existing monazite grains. While all Proterozoic gneiss samples outside of the roof zone are peraluminous and monazite-bearing, samples XG-2 and XG-7 from the roof zone are metaluminous, which may explain why they yielded only one monazite grain each. We did not obtain chemical analyses of rocks that did not yield monazite, so we don't know if the lack of monazite was a result of them being metaluminous. Mineralogical and petrographic evidence suggest large quantities of fluids moved through these rocks. As noted previously, at outcrop scale Proterozoic gneisses in the roof zone host abundant quartz-rich, ore-bearing veins. Petrographic study shows that gneiss samples contain large amounts of epidote and opaques and even some calcite, all minerals associated with hydrothermal alteration, often concentrated in micro-veins that cut across gneissic layering. Samples XG-2 and XG-7 have much higher CaO than other Proterozoic gneiss samples, possibly due to the presence of secondary calcite. In addition, samples XG-3 and XG-13 directly overlie, and XG-1 and XG-2 occur above the flank of, the Upper Searchlight unit and beneath the highly altered Miocene volcanic sequence. The overlying Miocene volcanic rocks contain the vast majority of the hydrothermal ore deposits in the area. It is likely that fluids released from the upper Searchlight unit caused much of the alteration in the augen orthogneiss samples, particularly XG-3 and XG-13. Evidence indicates that hydrothermal fluids were highly oxidized (Ludington and others, 2005). They may have reacted with monazite and converted Ce^{3+} to Ce^{4+}. Ce^{3+} is the primary LREE constituent of monazite, $(LREE)PO_4$, so any reactions that consume it are likely to affect the stability of monazite adversely. Monazite could also have simply dissolved in magmatic fluids because magmatic fluids become acidic as they cool (Brimhall and Crerar, 1987), and monazite is soluble in acidic fluids (Ayers and others, 2004; Poitrasson and others, 2004). Finally, Ca metasomatism could have changed the bulk composition of roof zone gneisses from peraluminous to metaluminous, causing monazite to become unstable.

Monazite grains from the Proterozoic gneiss display both patchy and concentric zoning (fig. 12). Monazite primary zones are more abundant than secondary zones (fig. 12), so they dominate the age spectra (figs. 14-15). Figure 13 shows that many monazite analyses are either normally or reversely discordant. Analyses showing normal discordance may result from Pb loss or mixing of concordant age populations. Analyses showing reverse discordance may result from uranium loss or result from

analytical error (Hawkins and Bowring, 1997). Most discordant analyses appear to plot on a single discordia with an upper intercept of 1646 ± 9 Ma and poorly defined lower intercept of 75 ± 61 Ma, but the high MSWD of 9.3 suggests that a single discordia cannot explain the isotopic variation, and that there may be more than two age populations. Most primary zone analyses plot near the upper intercept with discordia (fig. 13).

The discordia in figure 13 may represent a mixing line between zones with concordant ages corresponding to the upper and lower intercepts. However, that would not explain the many monazite grains that display reverse discordance. Reverse discordance may be a result of "mechanisms that involve exchange or fractionation of elemental U or elemental Pb," as suggested by Hawkins and Bowring (1997). The ~75 Ma age of the lower intercept is well within uncertainty of the age of intrusion of the Ireteba granite at 66 Ma. Thus it is plausible that intrusion of the Ireteba granite at 66 Ma disturbed the U-Pb system in monazite grains in the Proterozoic gneiss.

The percentage of discordant analyses is large because most analyses are mixtures of the dominant primary zones and secondary zones that are smaller than the analysis spot (fig. 12), and possibly other volumetrically minor age populations. LA-ICP-MS analysis yields no $^{207}Pb/^{206}Pb$ ages <1400 Ma, presumably because none of the secondary zones are large enough to be sampled exclusively by the 30 μm diameter laser spot (fig. 12), so the larger, older primary zones contribute the bulk of the radiogenic lead (table 6, fig. 13). Thus, we infer that the discordance in figure 13 primarily results from mixed analyses rather than Pb loss and that many if not all of the primary and secondary zones are concordant or reversely discordant. Although measured EMP ages are systematically too young (see Methods), secondary zones have an age peak centred at 65 Ma (fig. 15) that may correspond to the ~75 Ma lower intercept age on the concordia diagram (fig. 13) and the 66 Ma age of the Ireteba pluton. Unlike Ireteba monazite grains, Miocene deformation and magmatism had little effect on Proterozoic gneiss monazite grains.

The monazite upper intercept age of 1646 Ma (fig. 13) is 100 Ma younger and the monazite $^{207}Pb/^{206}Pb$ age is 65 Ma younger (fig. 14) than the ~1720 Ma peak in the zircon $^{207}Pb/^{206}Pb$ age spectra (fig. 14). The monazite ages are too young to represent the primary age of the Mojave terrane (>1.7 Ga). However, the ages may correspond to the 1.62 to 1.69 Ga intrusion of intermediate to felsic magma into the eastern Mojave terrane (Miller and Wooden, 1994) and agree well with a monazite metamorphic age of 1.67 Ga from the nearby Ivanpah Mountains in the Mojave terrane (Strickland and others, 2013). Thus, zircon may date magmatic crystallization of the Proterozoic gneiss protoliths, and primary zones in monazite may date a post-crystallization metamorphic event associated either with intrusion of nearby felsic magmas, or regional-scale metamorphism. Patchy secondary zones mostly formed in response to intrusion of the underlying Ireteba granite at ~66 Ma.

The Proterozoic gneiss monazite grains do not show a correlation between style or intensity of replacement zoning textures and distance from the Searchlight pluton contact. Furthermore, average monazite ages of samples collected along the transect show no systematic dependence on distance from the contact (fig. 17). If fluids or heat derived from the Searchlight pluton were responsible for altering country rock monazite, we would expect that monazite with the highest intensity of alteration, that is, the highest proportion of secondary zones and the youngest average ages, would be closest to the contact, and that the intensity of alteration would decrease and average age increase with increasing distance from the contact. However, that is not what we observe. The Proterozoic gneiss transect provides little evidence that hydrothermal fluids associated with intrusion of the Searchlight pluton infiltrated the wallrocks and caused monazite grains to recrystallize.

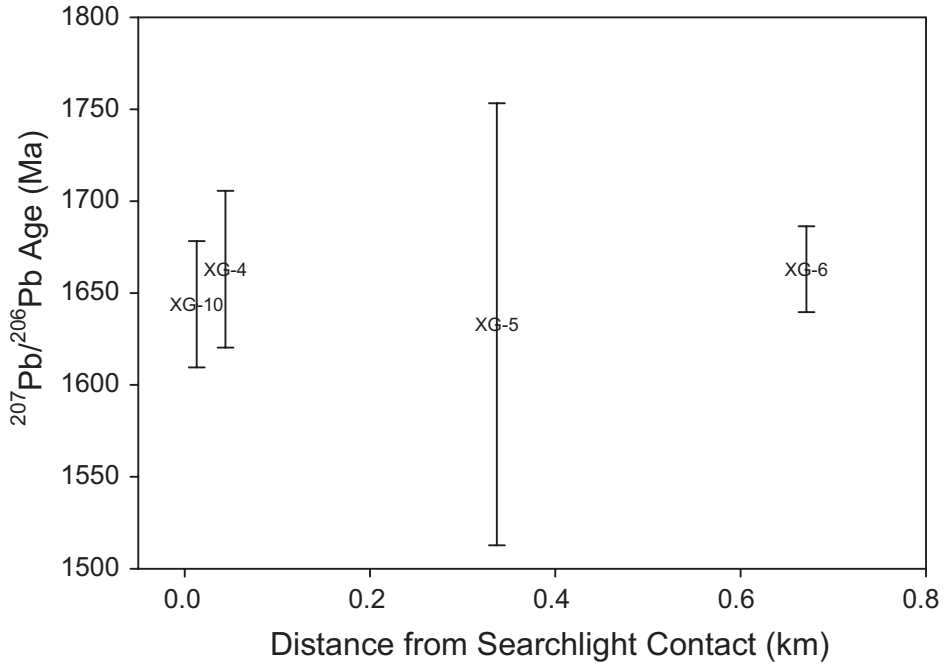

Fig. 17. Proterozoic gneiss $^{207}Pb/^{206}Pb$ monazite ages with one sigma error bars plotted as a function of distance from the Searchlight contact.

CONCLUSIONS

Monazite grains from Proterozoic gneiss and Ireteba granite country rocks of the Searchlight pluton have pervasive secondary patchy zoning. Patchy zoning in Ireteba monazite grains developed during or shortly after intrusion of the Searchlight pluton at ~16 to 17 Ma. Minor recrystallization of Proterozoic gneiss monazite grains led to growth of small scattered secondary domains with ages corresponding to intrusion of the underlying Ireteba granite, but monazite grains were mostly unaffected by the adjacent Searchlight intrusion, suggesting that patchy zoning predated the Searchlight pluton. None of the U-Pb ages of zircons from shallow Proterozoic gneiss samples corresponds to the timing of the Phanerozoic intrusions.

The Searchlight country rocks do not show evidence of strong hydrothermal alteration except in the roof zone. Rocks in the wall zone lack evidence of hydrothermal alteration of monazite and other minerals. In contrast, rocks in the roof zone are intensely altered and veined and host hydrothermal ore deposits, suggesting a focused release of fluid through the roof of the pluton. The upper Searchlight unit may have been responsible for most of the fluid release from the pluton. This fluid, once released, circulated through the Miocene volcanic rocks and Proterozoic gneiss in the shallow roof zone, possibly destroying pre-existing monazite grains. However, fluids were unable to penetrate into Proterozoic gneiss and Ireteba granite wallrocks, perhaps because they were deeper than the brittle- to ductile transition temperature and therefore impermeable. This prevented fluid alteration of monazite grains in wallrocks and the development of a well-defined contact metamorphic aureole.

Evidence for fluid alteration of monazite in the Ireteba granite is cryptic at best, with no clear shifts in whole rock hydrogen or oxygen isotope composition or in monazite oxygen isotope composition. Evidence suggests that monazite in the Ireteba

pluton partially recrystallized and developed patchy zoning in response to strain associated with Searchlight intrusion or Miocene tectonic activity. Use of patchy zoning in monazite as a diagnostic feature of hydrothermal alteration may be questionable.

ACKNOWLEDGMENTS

This material is based upon work supported by the National Science Foundation under Grant Nos. EAR-0126020 and EAR-9873626 to Ayers and Miller and EAR-0838391 to Ayers. Any opinions, findings, conclusions, or recommendations expressed in this material are those of the authors and do not necessarily reflect the views of the National Science Foundation. The ion microprobe facility at UCLA is partly supported by a grant from the Instrumentation and Facilities Program, Division of Earth Sciences, National Science Foundation. Thanks to Steve Ludington (USGS) for sharing GIS data and for help in the field. Reviews by Mike Williams and an anonymous reviewer helped to improve the manuscript.

Appendix

Table A1

Monazite chemical U,Th-Pb ages measured on Cameca SX-100

Anal. #	Sample ID	Sample	Age (Ma)	1 sigma	MC error
9	xg9mon4	XG-9	1377.4	9.1	10.1
10	xg9mon4	XG-9	1502.2	11.9	12.8
11	xg9mon4	XG-9	1572.4	14.8	15.6
12	xg9mon5	XG-9	1539.4	14.4	15
13	xg9mon5	XG-9	1497.8	17.1	17.9
14	xg9mon5	XG-9	1477.1	14.0	15.1
15	xg9mon5	XG-9	1166.8	8.8	9.5
16	xg9mon2	XG-9	55.8	7.7	5.9
17	xg9mon2	XG-9	1377.4	10.7	11.8
18	xg9mon2	XG-9	1299.6	8.6	9.3
19	xg9mon2	XG-9	1407.9	11.8	12.7
20	xg9mon2	XG-9	1483.7	14.8	15.7
21	xg9mon2	XG-9	1496.8	15.3	16.1
22	xg9mon2	XG-9	63.9	1.7	1.5
23	xg9mon3	XG-9	1368.4	10.4	11.7
24	xg9mon3	XG-9	1399.0	10.5	11.5
25	xg9mon3	XG-9	1479.8	14.8	15.7
26	xg9mon3	XG-9	1490.8	14.5	15.3
27	xg9mon3	XG-9	1486.9	17.7	18.9
28	xg9mon3	XG-9	1488.3	16.9	18
29	xg9mon3	XG-9	1430.4	14.6	15.8
30	xg9mon3	XG-9	1295.1	14.6	15.8
31	xg9mon3	XG-9	1493.9	14.9	15.7
32	xg9mon9	XG-9	1318.5	8.8	9.7
33	xg9mon9	XG-9	1305.8	8.7	9.5
34	xg9mon9	XG-9	1353.0	10.8	12.1
35	xg9mon9	XG-9	1369.6	10.8	12.1
36	xg9mon9	XG-9	1490.4	14.2	15.1
37	xg9mon9	XG-9	1481.9	13.6	14.1
38	xg9mon9	XG-9	1480.0	16.3	17.4
39	xg9mon9	XG-9	1431.8	16.4	17.6
40	xg9mon9	XG-9	1393.6	14.0	14.9
41	xg9mon9	XG-9	1412.2	13.6	14.7
42	xg9mon9	XG-9	1383.5	11.2	12.0
43	xg9mon9	XG-9	1439.7	13.4	14.4
44	xg11mon1	XG-11	915.6	12.4	13
45	xg11mon1	XG-11	1186.0	13.4	14.5
46	xg11mon1	XG-11	1162.7	15.7	16.8
47	xg11mon1	XG-11	1180.2	15.9	16.7
48	xg11mon1	XG-11	45.5	4.3	3.3
49	xg11mon1	XG-11	33.3	4.0	3.9
50	xg11mon1	XG-11	1141.6	14.3	15.4
51	xg11mon1	XG-11	20.0	3.0	4.2
52	xg11mon2	XG-11	1203.1	14.5	15.5
53	xg11mon2	XG-11	1138.1	14.4	15.3
54	xg11mon2	XG-11	1155.5	14.3	15.3
55	xg11mon2	XG-11	1102.9	11.8	12.6
56	xg11mon2	XG-11	987.1	11.3	11.7
57	xg11mon2	XG-11	1214.2	13.6	14.3
58	xg11mon2	XG-11	1121.0	13.4	14.1
59	xg11mon2	XG-11	1087.0	12.7	13.2
60	xg11mon2	XG-11	954.6	12.1	12.9
61	xg11mon3	XG-11	90.9	7.5	4.8
62	xg11mon3	XG-11	421.2	14.0	14.1
63	xg11mon3	XG-11	1219.7	19.3	20.9
64	xg11mon3	XG-11	1065.1	18.8	20.3
65	xg11mon3	XG-11	1192.6	17.7	18.4
66	xg11mon3	XG-11	1166.0	18.9	20.0
67	xg11mon3	XG-11	865.5	17.4	18.3
68	xg11mon3	XG-11	1198.1	15.9	17.1
69	xg11mon3	XG-11	1110.0	18.9	19.6
70	xg11mon3	XG-11	1187.9	19.2	20.3
71	xg11mon4	XG-11	1215.5	17.9	19.4
72	xg11mon4	XG-11	1020.5	17.7	18.8
73	xg11mon4	XG-11	1336.0	19.2	20.7
74	xg11mon4	XG-11	1007.2	18.9	19.7
75	xg11mon4	XG-11	1188.5	15.1	16.1
76	xg11mon4	XG-11	1187.0	15.3	16.5
77	xg11mon4	XG-11	1279.0	14.2	15.3
78	xg11mon4	XG-11	1224.1	14.7	15.7
79	xg11mon4	XG-11	1414.9	13.2	14.1
80	xg11mon4	XG-11	1396.1	12.4	13.4
81	xg11mon4	XG-11	1182.7	10.9	11.4
82	xg11mon4	XG-11	1193.7	11.3	11.9
83	xg11mon4	XG-11	1278.5	19.0	20.0
84	xg11mon4	XG-11	1307.2	17.2	18.0
85	xg10mon9	XG-10	940.7	6.9	7.6
86	xg10mon9	XG-10	1415.2	15.5	16.7
87	xg10mon9	XG-10	1400.1	14.6	15.5
88	xg10mon9	XG-10	1328.4	14.2	15.2
89	xg10mon9	XG-10	1429.7	22.5	24.5
90	xg10mon9	XG-10	1435.6	18.5	20.1
91	xg10mon9	XG-10	1454.9	21.8	23.7
92	xg10mon9	XG-10	1406.2	13.0	14.1
93	xg10mon9	XG-10	1401.6	14.0	15.2
94	xg10mon9	XG-10	1443.9	13.8	14.8
95	xg10mon9	XG-10	1477.9	15.4	16.2
96	xg10mon9	XG-10	1440.7	14.6	15.4
97	xg10mon9	XG-10	1428.5	12.7	13.4
98	xg10mon9	XG-10	1219.6	11.9	12.5
99	xg10mon9	XG-10	1469.2	19.0	20.3
100	xg10mon9	XG-10	1438.0	17.9	19.4
101	xg10mon9	XG-10	1375.3	12.8	13.7
102	xg10mon10	XG-10	1441.5	24.7	26.7
103	xg10mon10	XG-10	1388.3	25.3	27.1
104	xg10mon10	XG-10	1456.6	19.9	21.3
105	xg10mon10	XG-10	1406.0	18.8	20.0
106	xg10mon10	XG-10	1381.7	12.5	13.1
107	xg10mon10	XG-10	1392.1	12.2	12.9
108	xg10mon10	XG-10	1398.6	14.8	15.7
109	xg10mon10	XG-10	1434.6	15.0	16.1
110	xg10mon10	XG-10	1470.8	23.5	25.1
111	xg10mon10	XG-10	1446.1	26.9	28.5
112	xg10mon8	XG-10	1469.3	20.0	21.4
113	xg10mon8	XG-10	1406.3	19.4	20.9
114	xg10mon8	XG-10	1401.6	16.4	17.5
115	xg10mon8	XG-10	1378.3	15.8	16.8
116	xg10mon8	XG-10	1433.3	17.7	19.1
117	xg10mon8	XG-10	948.2	17.7	18.7
118	xg10mon8	XG-10	1438.1	18.2	19.4
119	xg10mon8	XG-10	1406.4	17.9	19.3
120	xg10mon8	XG-10	1300.7	16.7	17.7
121	xg10mon8	XG-10	1353.2	17.5	18.5
122	xg12mon2	XG-12	44.6	4.3	5.5
123	xg12mon2	XG-12	103.1	7.1	5.4
124	xg12mon2	XG-12	1416.2	15.7	16.8
125	xg12mon2	XG-12	1439.0	15.7	16.9
126	xg12mon2	XG-12	1246.0	12.0	12.4
127	xg12mon2	XG-12	920.4	10.2	10.6
128	xg12mon2	XG-12	1421.0	12.5	13.3
129	xg12mon2	XG-12	1411.9	12.6	13.7
130	xg12mon4	XG-12	54.5	5.6	4.4
131	xg12mon4	XG-12	79.0	6.5	4.5
132	xg12mon4	XG-12	57.3	5.2	5.7

TABLE A1
(continued)

Anal. #	Sample ID	Sample	Age (Ma)	1 sigma	MC error
133	xg12mon4	XG-12	1306.0	15.8	16.9
134	xg12mon4	XG-12	1410.1	15.7	16.7
135	xg12mon4	XG-12	13.7	0.8	0.1
136	xg12mon8	XG-12	32.6	3.2	2.6
137	xg12mon8	XG-12	47.1	4.6	4.6
138	xg12mon8	XG-12	64.7	5.5	3.5
139	xg12mon8	XG-12	55.7	5.1	5.2
140	xg12mon8	XG-12	1299.1	11.5	12.4
141	xg12mon8	XG-12	1323.3	11.6	12.5
142	xg4mon5	XG-4	1439.7	15.7	16.9
143	xg4mon5	XG-4	1395.8	15.9	17.3
144	xg4mon5	XG-4	1451.2	18.7	20.4
145	xg4mon5	XG-4	1414.1	19.4	20.7
146	xg4mon5	XG-4	1320.8	9.8	11.0
147	xg4mon5	XG-4	1012.3	10.3	11.0
148	xg4mon5	XG-4	1303.5	16.6	17.8
149	xg4mon2	XG-4	1270.5	9.2	10.2
150	xg4mon2	XG-4	1296.1	9.4	10.4
151	xg4mon2	XG-4	1423.1	13.7	14.8
152	xg4mon2	XG-4	1415.4	14.0	15.4
153	xg4mon2	XG-4	342.4	17.1	18.3
154	xg4mon2	XG-4	67.7	8.9	3.7
155	xg4mon7	XG-4	1475.3	14.8	16.1
156	xg4mon7	XG-4	1396.4	16.7	17.8
157	xg4mon7	XG-4	1462.4	16.2	17.5
158	xg4mon7	XG-4	1498.6	15.8	17.2
159	xg4mon7	XG-4	1381.9	10.3	11.1
160	xg4mon7	XG-4	1425.3	10.9	11.8
161	xg4mon7	XG-4	1152.7	7.4	8.0
162	xg4mon7	XG-4	1141.6	7.4	8.2
163	xg4mon7	XG-4	1320.2	9.7	10.6
164	xg5mon1	XG-5	1440.0	15.2	16.6
165	xg5mon1	XG-5	1405.8	14.8	16.3
166	xg5mon1	XG-5	1378.4	14.7	16.0
167	xg5mon1	XG-5	1382.2	14.2	15.5
168	xg5mon1	XG-5	1414.8	12.5	13.4
169	xg5mon1	XG-5	1434.3	15.1	16.4
170	xg5mon1	XG-5	1433.1	14.5	15.8
171	xg5mon1	XG-5	10.8	0.3	0.3
172	xg5mon3	XG-5	68.5	1.2	1.2
173	xg5mon3	XG-5	1227.3	9.8	10.2
174	xg5mon3	XG-5	1194.7	11.8	12.3
175	xg5mon3	XG-5	1227.8	12.6	13.0
176	xg5mon3	XG-5	292.6	8.5	8.8
177	xg5mon3	XG-5	1201.4	10.5	10.9
178	xg5mon4	XG-5	784.1	6.2	6.7
179	xg5mon4	XG-5	945.2	7.7	8.3
180	xg5mon4	XG-5	1437.2	24.5	26.7
181	xg5mon4	XG-5	1415.9	18.3	19.6
182	xg5mon4	XG-5	1382.9	17.5	19.1
183	xg5mon4	XG-5	1437.2	17.3	18.6
184	xg5mon4	XG-5	1355.4	16.6	18.1
185	xg5mon4	XG-5	1385.6	18.1	19.4
186	xg6mon10	XG-6	1396.5	11.9	12.7
187	xg6mon10	XG-6	1323.1	10.4	11.3
188	xg6mon10	XG-6	1388.1	15.9	17.2
189	xg6mon10	XG-6	1400.8	13.0	13.9
190	xg6mon10	XG-6	1461.5	16.6	18.0
191	xg6mon6	XG-6	1295.5	10.7	11.5
192	xg6mon6	XG-6	1424.5	18.0	19.7
193	xg6mon6	XG-6	1418.7	16.8	18.5
194	xg6mon6	XG-6	1311.1	11.8	12.6
195	xg6mon6	XG-6	1355.6	17.0	18.5
196	xg6mon6	XG-6	1472.3	17.8	19.2
197	xg6mon6	XG-6	1381.0	12.9	14.1
198	xg6mon6	XG-6	1335.6	10.9	11.8
199	xg6mon6	XG-6	1423.5	15.1	16.5
200	xg6mon7	XG-6	1399.7	16.7	18.3
201	xg6mon7	XG-6	1472.9	17.2	18.6
202	xg6mon7	XG-6	1454.9	17.7	18.8
203	xg6mon7	XG-6	1456.9	16.3	17.6
204	xg6mon7	XG-6	1404.7	13.7	14.9
205	xg6mon7	XG-6	89.1	6.6	7.4
206	xg6mon7	XG-6	94.3	7.9	7.9
207	xg2mon1	XG-2	1334.1	8.7	9.7
208	xg2mon1	XG-2	1296.2	8.7	9.6
209	xg2mon1	XG-2	1269.2	8.4	9.3
210	xg2mon1	XG-2	872.8	6.5	6.9
211	xg2mon1	XG-2	849.7	6.4	6.9
212	xg2mon1	XG-2	412.4	3.5	3.7
213	xg2mon1	XG-2	460.8	3.3	3.6
214	xg7mon1	XG-7	6.6	2.7	10.6
216	xg7mon1	XG-7	80.6	16.5	13.0

Table A2

Monazite element concentrations in parts per million as measured on Cameca SX-100

spot#	sample	grain	Si	P	Ca	Y	La	Ce	Pr	Nd	Sm	Gd	Th	U	Tb	Dy	Er	Pb avg
9	XG-9	4	13231	111659	12024	902	71005	192940	25308	110056	18951	7068	113185	2150	858	149		10814
10	XG-9	4	7243	121029	10278	936	87990	220050	27456	111289	19326	10097	67999	2172	345	605	270	7224
11	XG-9	4	772	130961	9185	19721	114200	234236	25684	90730	16451	13724	25534	10317	1515	6660	1704	5315
12	XG-9	5	735	131153	9270	22945	108663	230276	24985	96038	17595	15051	25072	11341	1945	7881	2269	5352
13	XG-9	5	631	130288	8595	9407	110916	240261	26336	102507	19989	16959	26632	5498	2137	5414	650	3947
14	XG-9	5	1616	127177	11708	3631	102508	232816	26918	104129	19954	14712	44157	4259	1198	2091	282	5312
15	XG-9	5	12932	111924	10083	839	74430	201261	26076	113776	19732	7341	98557	2019	647	265	292	7866
16	XG-9	2	770	131653	4858	18260	122514	252462	26524	97969	17809	15126	20441	324	1848	6976	1454	68
17	XG-9	2	8109	121493	12082	1057	75191	211680	27785	119451	20674	6736	79162	1850	433	307	70	7676
18	XG-9	2	16250	106944	10842	375	69023	190398	24678	107430	17445	7813	117235	3530		380	176	10845
19	XG-9	2	6096	123684	11181	1047	86639	223693	27433	116304	20300	8816	65852	1889	296	225		6553
20	XG-9	2	580	131249	9092	20439	115958	234951	25005	93825	15677	13966	24065	10380	1720	6911	1950	4904
21	XG-9	2	1588	130135	8330	13074	108076	238156	26812	102553	18667	13659	29129	7409	1280	5324	920	4625
22	XG-9	2	27976	100217	1708	79105	65210	137964	14710	60292	9252	18060	91931	35233	3070	19769	6859	652
23	XG-9	3	10170	118927	10154	361	81702	211218	27136	110636	19516	7679	82538	2171	447	453	18	8092
24	XG-9	3	10287	118991	10145	452	81462	213284	27085	110333	19391	8959	82089	2117	652	312	147	8193
25	XG-9	3	627	133581	9117	22889	110849	232805	24979	93427	16504	14642	24193	10284	1466	7513	2102	4871
26	XG-9	3	737	132069	9295	22101	109856	230911	25005	95152	16845	14629	24829	10661	1779	7314	1877	5077
27	XG-9	3	769	131645	8088	7714	113114	243438	26779	103684	19778	16561	25486	5135	1493	4669	403	3761
28	XG-9	3	565	132244	8650	9317	112071	241216	26370	102119	19434	16874	25952	6142	2007	5297	387	4016
29	XG-9	3	4848	125919	6852	3968	109494	241188	27548	103086	17242	11109	44710	2147	1400	2492	50	4730
30	XG-9	3	4301	125021	6578	4415	111722	244796	26534	103881	17954	11405	41549	2301	748	2426	528	4032
31	XG-9	3	598	130727	9157	20255	113086	236048	25650	94782	16456	14105	24067	10148	2151	6991	1854	4860
32	XG-9	9	15246	111962	12668	774	68939	188124	24287	108851	17881	7159	115637	2445	349	333	39	10688
33	XG-9	9	16085	110459	12083	752	67342	183311	24537	105690	17666	6365	119051	2420		441	212	10802
34	XG-9	9	8772	121495	10108	496	86566	218833	26822	114367	19732	8882	74843	2036	765	373		7318
35	XG-9	9	8884	123255	10351	534	83896	218490	26937	114302	19597	7866	75799	1938	358	590	72	7465
36	XG-9	9	900	133462	10100	20411	109272	230234	25255	94549	15530	14301	30644	9149	1880	7055	1983	5268
37	XG-9	9	951	133694	10342	22417	104378	226255	24927	95988	17593	14369	29013	11606	2004	7659	2260	5630
38	XG-9	9	1444	131693	8679	3766	111906	245884	26988	105588	19123	13915	31883	4578	1546	2537		4186
39	XG-9	9	1431	130872	8536	3393	112457	246536	27288	105710	20470	14883	31384	4343	1091	2371	216	3945
40	XG-9	9	3409	129592	9868	928	99392	238244	27976	111585	19751	10969	47783	2163	454	296	9	4901
41	XG-9	9	3734	127422	10189	824	99231	235888	27572	112014	20360	10642	50543	2224	97	382	(29)	5279
42	XG-9	9	7437	122934	11278	904	89593	219423	26142	108637	19247	9946	72177	2241	849	779	169	7204
43	XG-9	9	3687	128730	9663	6632	102253	232526	26019	103698	19706	13435	46278	4513	1560	3292	432	5503

Table A2
(continued)

spot#	sample	grain	Si	P	Ca	Y	La	Ce	Pr	Nd	Sm	Gd	Th	U	Tb	Dy	Er	Pb avg
44	XG-11	1	6057	121230	5466	1814	109575	250889	28585	107296	13623	4733	49426	818	157	743	219	3124
45	XG-11	1	6490	122556	5163	999	109405	252080	27744	108431	13651	5756	49587	727	607	347		4066
46	XG-11	1	3581	126686	7128	3877	120544	250380	27022	96221	15763	11056	37746	1258	861	2590	80	3141
47	XG-11	1	3417	127477	6332	3941	122680	251780	26820	96924	15443	9828	37713	1034	1151	2176	115	3141
48	XG-11	1	2226	128308	9071	17649	117789	234237	24794	91816	12687	10904	44025	1066	1199	6286	1417	118
49	XG-11	1	2952	126942	8350	11586	113997	243582	26147	96936	14428	9361	42204	1275	674	4216	904	99
50	XG-11	1	4066	126484	5965	5263	111688	242877	27745	103647	18463	13097	38995	3010	1418	3110	98	3498
51	XG-11	1	3155	127703	7899	7009	115895	245597	26713	99007	13907	9504	44123	1570	651	2820	358	81
52	XG-11	2	4951	124516	5377	3365	124516	253931	25992	97171	12649	7692	42205	1551	349	1386	288	3668
53	XG-11	2	3257	127290	6935	2877	116839	247412	27859	102772	17885	11451	37566	3404	1343	2113		3429
54	XG-11	2	2652	128356	7638	5162	115793	242900	27603	102104	17850	13732	36518	4105	1604	3299	272	3566
55	XG-11	2	8156	117370	4776	92	113510	247398	27199	103374	12528	4136	57576	893	97	139	20	4346
56	XG-11	2	8098	119208	4993	647	112803	247024	27946	103681	12208	4789	58779	757	388	47	65	3856
57	XG-11	2	6658	123172	5091	438	116472	249945	27868	103663	12463	4862	49551	658	241	265	248	4079
58	XG-11	2	6599	119962	4921	450	116342	251034	27559	104840	12965	5054	49509	409	71	216	166	3791
59	XG-11	2	6095	114019	5589	837	115733	249934	28380	104468	13155	5085	51692	915	613	722	85	3835
60	XG-11	2	6827	122606	5563	481	115683	248928	28135	104038	12895	4377	52295	581		220	171	3367
61	XG-11	3	1126	131852	7301	21915	113642	240855	26250	94975	15843	12135	28734	3736	883	6941	2051	166
62	XG-11	3	1616	128892	6287	15178	115963	249306	27099	99092	15603	11422	28093	2643	834	4675	1374	924
63	XG-11	3	1474	131318	6444	9453	122748	254502	26983	97807	15369	9323	25296	2549	1088	3490	511	2538
64	XG-11	3	1205	131321	6432	10127	124920	255649	27918	97315	14631	9505	24815	2614	1446	3414	953	2226
65	XG-11	3	1876	128860	5562	15223	109121	252480	26987	101269	17834	13451	24228	4270	1291	5109	1277	2642
66	XG-11	3	2905	126477	4821	4208	122360	261915	27674	101498	15483	9120	29111	1079	657	2187	429	2424
67	XG-11	3	2723	128856	4868	7804	118255	257763	27760	103184	16573	10863	27909	1857	793	2938	567	1866
68	XG-11	3	2253	128271	6080	11943	111221	247851	27192	102431	18003	13711	27334	5325	1176	4595	1052	3226
69	XG-11	3	1892	128123	4902	10643	113711	257929	28589	102604	18519	12930	22548	3673	884	4077	1084	2277
70	XG-11	3	2132	129577	5006	8662	113244	256818	28945	104420	18290	12410	24249	2900	1330	3617	755	2422
71	XG-11	4	3342	126534	4666	671	107584	268479	30142	118580	16307	5697	30240	1957	665	254		2859
72	XG-11	4	2978	126180	4597	920	107889	266052	30470	116372	16104	5709	29004	1962		201	118	2273
73	XG-11	4	3171	128411	4398	501	107080	268498	30703	116857	16331	5271	28590	1714	569	343	122	2875
74	XG-11	4	1799	129822	4330	1727	123901	272354	29767	102717	15406	7837	19028	5183	338	994	260	2064
75	XG-11	4	5062	126033	5165	509	101074	255589	30950	117192	15720	5051	41691	735	451	64	150	3500
76	XG-11	4	4809	124175	5120	673	100104	257938	30394	119641	16853	5396	40782	738	303	207		3324
77	XG-11	4	4226	127125	6722	6005	106540	245471	27681	106110	18013	12616	41113	3253	939	2948	124	4197
78	XG-11	4	5541	125411	5332	704	99855	252982	29968	114224	16383	6612	43852	994	595	297	214	3817
79	XG-11	4	2262	130923	11700	9724	112062	231146	24346	90524	17295	13844	44040	5987	1599	4197	380	5502

Table A2

(continued)

spot#	sample	grain	Si	P	Ca	Y	La	Ce	Pr	Nd	Sm	Gd	Th	U	Tb	Dy	Er	Pb avg
80	XG-11	4	2390	129364	12273	9658	110091	227909	24165	92624	16716	13671	47631	6851	1535	4695	508	5971
81	XG-11	4	8898	113798	6601	499	92456	234973	28387	113826	16187	5422	68767	1283	287	149	98	5570
82	XG-11	4	8502	116760	6187	367	93106	237322	28827	112693	15913	5570	64349	1417	332	302	90	5282
83	XG-11	4	2033	127678	5447	2544	120360	262324	27547	103273	17390	10215	25406	3206	769	1352	323	2766
84	XG-11	4	2270	127807	5492	2136	118512	262159	27198	102637	16891	9492	24984	5353	955	1355	241	3206
85	XG-10	9	24639	95106	2106	855	73475	195050	24984	103170	14767	6435	130777	1913	343	278		8400
86	XG-10	9	6774	121698	3535	415	107297	254762	30161	118368	14870	5154	43969	512	627	183	76	4220
87	XG-10	9	7524	121175	3616	441	104661	253580	29737	116098	14075	4858	47794	575	318	282	146	4589
88	XG-10	9	7601	121890	3592	569	103806	251423	30364	116759	14568	6279	48505	462		141	165	4412
89	XG-10	9	2434	128885	3979	114	119175	266983	29843	111686	20649	8919	22340	2104	319	162	237	2627
90	XG-10	9	3069	128326	5120	2306	117586	252931	28394	107951	20137	12947	29673	2282	738	1794	188	3359
91	XG-10	9	3727	126564	2943	1851	112638	261493	30353	115066	18922	10266	25797	1060	685	1156	150	2779
92	XG-10	9	9774	118564	3255	443	103335	245199	29682	112623	15329	5303	57497	878	169	502		5589
93	XG-10	9	8254	120171	3389	477	102831	251662	29107	112853	14564	5436	50686	660	398	542	271	4910
94	XG-10	9	8326	119768	3657	723	104873	245834	29335	111366	15112	7978	52582	1036	424	450	164	5172
95	XG-10	9	1419	131727	8073	15426	119361	238972	25617	95065	15530	13386	24800	8936	1379	5805	837	4551
96	XG-10	9	2706	126669	7688	11377	115397	242601	26410	103339	17184	11929	28444	8710	1027	4487	1060	4704
97	XG-10	9	9087	114408	4083	917	96019	240459	29231	120852	15266	6325	60359	920	257	472	195	5816
98	XG-10	9	9813	116234	4133	1064	92013	237604	30435	119603	15433	6683	61048	636	511	653	330	5020
99	XG-10	9	2965	127148	5255	2395	116238	251391	28746	105290	20392	13598	28499	2464	1200	1737		3320
100	XG-10	9	3035	126212	5759	3144	115330	249471	27941	106380	20990	14998	29813	2931	928	1910	206	3518
101	XG-10	9	9825	116864	3416	439	101720	243545	28990	113079	15401	6002	58560	844	404	268	66	5556
102	XG-10	10	2456	128805	3432	1623	109808	274701	31275	117679	16159	8171	21482	1073	409	948	18	2302
103	XG-10	10	2136	126965	3557	1687	113112	275671	31318	112836	16028	8325	20248	1269	469	1062	54	2144
104	XG-10	10	3880	125083	3888	1494	104570	261196	31499	119933	17163	8041	30116	826	784	951		3020
105	XG-10	10	4182	123945	3952	1389	102062	262644	31058	121601	16745	8194	32216	797	779	738	48	3186
106	XG-10	10	9816	115192	3970	779	89884	237353	30102	121330	16302	5989	61213	761	235	412		5721
107	XG-10	10	10036	113428	4335	543	87299	233553	30195	127668	16438	5361	63500	892	4	187		6027
108	XG-10	10	7064	118337	3857	630	93040	245650	32039	125461	18695	6582	46445	863	786	562	81	4477
109	XG-10	10	7041	117944	3637	521	93881	247967	31662	128326	17895	6220	45554	891	638	303	201	4519
110	XG-10	10	1745	125390	5333	1586	104900	265517	30677	121058	18716	8249	24239	563	325	879		2482
111	XG-10	10	1337	127868	5017	1612	105668	268677	32209	118513	18989	8232	20211	632	158	590	272	2051
112	XG-10	8	4152	124942	3154	1663	114701	256187	29298	115132	21581	11874	28550	1403	1123	1307	174	3096
113	XG-10	8	4038	124462	3276	2078	114654	253878	29467	113795	22184	13580	28980	1583	1236	1545	51	3035
114	XG-10	8	6172	122559	3380	793	103186	257955	30304	120054	16049	6581	40158	539	623	607	90	3835

Table A2
(continued)

spot#	sample	grain	Si	P	Ca	Y	La	Ce	Pr	Nd	Sm	Gd	Th	U	Tb	Dy	Er	Pb avg
116	XG-10	8	2118	126583	6214	10596	115610	240816	27031	102772	20078	17900	26896	4216	1915	5691	499	3508
117	XG-10	8	2720	125341	4872	3075	114354	249329	28986	110679	22280	15069	28184	2000	820	2258	226	2054
118	XG-10	8	2302	126193	5880	7251	116140	248124	27361	103542	20091	16308	27115	3685	1029	4383	279	3396
119	XG-10	8	2303	125461	6035	7624	114840	242933	27458	105197	21639	16506	26916	3905	1671	4017	130	3432
120	XG-10	8	5154	120189	3650	387	102480	257513	31640	123721	17833	6581	36733	1006	591	231	72	3380
121	XG-10	8	4952	121769	3528	424	102635	256970	31694	122964	16957	6159	34978	896	243	195		3312
122	XG-12	2	962	126235	8413	23906	106920	232733	26079	99701	15512	14807	33625	2513	1255	7270	2339	144
123	XG-12	2	1318	127903	8696	23196	106812	230538	26335	99519	16534	13109	36130	1862	1668	7019	2118	222
124	XG-12	2	3378	124466	7264	1987	113701	247189	27907	107248	17656	10702	38798	2379	1240	1404	126	4152
125	XG-12	2	3327	124180	7404	2411	112272	245852	28478	107470	17057	12146	39102	2202	810	1705	324	4200
126	XG-12	2	1766	124802	10839	6805	108126	236932	27315	101383	18002	12739	36832	10924	1293	3004	330	5084
127	XG-12	2	1087	126878	12152	10000	105084	232413	26595	99336	17567	12864	38287	12602	1556	3982	641	4073
128	XG-12	2	6255	117510	8997	1562	90874	228357	28371	114217	19138	8451	60582	1327	498	749	50	5932
129	XG-12	2	5689	117788	9208	1504	93942	233484	29111	114247	17577	8597	58703	1577	1062	957	149	5851
130	XG-12	4	1679	126259	6170	21465	115041	239500	26879	99447	14845	12676	30253	543	1676	6574	1911	98
131	XG-12	4	1454	127359	8139	19907	111573	238338	26963	99404	15317	13202	34672	2375	1741	6042	1795	162
132	XG-12	4	1652	127658	7994	20951	109642	235407	26222	97753	15093	12103	36374	1210	899	5963	1980	159
133	XG-12	4	3557	122639	6398	2378	114515	251414	27828	105228	16254	10146	38383	1510	891	1278	69	3625
134	XG-12	4	3988	120473	6394	2431	114153	249602	27793	106127	16420	9574	40322	1537	783	1290	313	4053
135	XG-12	4	22323	85043	7545	11016	86793	182012	19765	69758	11691	11594	148532	6534	1293	4591	1004	87
136	XG-12	8	1305	127942	11626	17163	105711	231724	26179	96415	15111	11600	42838	6049	1288	4469	1670	104
137	XG-12	8	1001	127416	8218	22272	107385	235767	27197	97812	16046	12089	32741	2751	1640	6364	2168	120
138	XG-12	8	1755	126846	8555	21194	110688	236528	26724	97525	15604	12149	36786	2268	2016	6331	1989	138
139	XG-12	8	1427	127923	8253	21033	107566	236188	27035	99867	16230	12593	35116	2059	1561	5613	2255	149
140	XG-12	8	9143	111793	6137	1169	97557	234414	27896	111334	16434	7588	65869	1551	237	624	55	5940
141	XG-12	8	9087	110094	5928	613	95765	234345	28489	111469	16250	8233	65807	1331	309	579		5985
142	XG-4	5	2902	125243	6526	8601	97283	233559	28903	116509	23382	17531	31029	5592	1811	4322	351	4281
143	XG-4	5	2674	124147	6279	9370	99381	233902	28770	115942	23881	18896	28837	5660	1552	4470	503	3956
144	XG-4	5	1422	127384	5661	23553	105974	227792	26778	103887	21290	22181	21231	5085	2997	10499	1581	3261
145	XG-4	5	1415	127604	5236	22177	109054	232723	26428	103167	21497	21480	20229	4723	2394	10195	1301	2996
146	XG-4	5	13635	108266	7132	2450	67872	199649	27786	125441	22710	9482	88501	2429	545	957	359	8382
147	XG-4	5	10087	119295	8196	5524	70606	208333	28944	124061	22449	12748	61004	3766	1103	2469	523	4599
148	XG-4	5	2177	124921	5965	11758	102512	230952	27907	112003	24023	20999	26241	5410	1729	5836	553	3410
149	XG-4	2	15336	106625	6139	1134	73952	203301	27571	118539	20567	7698	96666	2579	192	766	291	8742
150	XG-4	2	15603	106513	6163	1136	72764	205551	27866	119339	20037	7729	94815	2426	825	510	301	8788

Table A2

(continued)

spot#	sample	grain	Si	P	Ca	Y	La	Ce	Pr	Nd	Sm	Gd	Th	U	Tb	Dy	Er	Pb avg
151	XG-4	2	4827	121731	7844	1990	99074	233382	28138	115396	21293	11760	48579	2465	591	1181	240	5179
152	XG-4	2	4386	122252	7900	2072	102166	239829	28632	112710	20717	11052	46614	2302	1042	1126	233	4916
153	XG-4	2	1559	127414	4492	15160	119669	249146	27026	102419	18685	14198	23081	611	1426	5855	1372	588
154	XG-4	2	1029	129711	4466	17159	123006	247820	27123	98211	17707	14806	21001	248	1647	6474	1628	64
155	XG-4	7	4473	124376	6027	21772	99826	220497	26784	104969	20488	19940	38338	4162	2398	9465	1489	4738
156	XG-4	7	4511	123005	3624	8320	103259	235639	28434	116193	23955	18001	31453	3545	1295	5045	326	3668
157	XG-4	7	1566	128865	7552	22848	104025	225991	25958	99931	20458	19827	28029	5711	2434	9641	1628	4082
158	XG-4	7	1905	127160	7682	24000	101061	222847	25305	102828	20350	21673	29606	5797	2721	9964	1736	4398
159	XG-4	7	10753	114356	8864	3824	81713	205092	27284	115211	20888	11214	79094	4880	576	1915	127	8392
160	XG-4	7	9336	112975	8690	6679	84859	207821	26890	112284	21665	13858	69401	5193	1062	3264	430	7784
161	XG-4	7	23394	88066	6450	1953	58772	171116	23500	106940	19761	8125	143301	3499	221	834	332	11493
162	XG-4	7	25201	92481	6257	1887	59393	170942	24681	109199	19094	7671	142696	3443	872	897	104	11544
163	XG-4	7	13406	107188	6852	2482	76608	204525	28100	118075	22457	10260	87398	4226	743	1452	72	8548
164	XG-5	1	2529	124440	8773	10218	114271	252487	26666	93744	12980	7936	39843	2514	414	2374	658	4359
165	XG-5	1	2793	125094	8850	10396	114955	249189	26671	94197	13178	7720	40974	2548	959	2553	620	4475
166	XG-5	1	6961	119696	3640	4388	119495	257496	27172	94360	12014	6118	45515	952	700	1508	270	4356
167	XG-5	1	7801	119047	3419	3833	122455	255157	27038	93880	11303	6040	48688	718	483	1252	240	4658
168	XG-5	1	10021	114522	3706	3720	113422	245983	26079	93568	12826	6403	60865	1069	10	1407	291	5929
169	XG-5	1	4897	121649	6519	4732	109359	252777	28147	97718	16185	9554	43853	1256	780	1849	128	4458
170	XG-5	1	5345	121006	6364	4099	105158	243928	28758	102673	19107	11948	46028	1599	991	2244	219	4777
171	XG-5	1	77043	16665	2547	9405	11683	25590	2504	11554	1754	2583	388485	45150	465	2329	598	348
172	XG-5	3	15877	78690	9623	14425	63057	146767	11941	29674	3808	5010	131358	139732	865	5028	1655	1912
173	XG-5	3	993	128964	14698	22378	168539	214574	15638	39331	5747	6934	39374	20270	1479	6483	1964	7131
174	XG-5	3	573	129404	9127	19214	180120	235212	18169	46081	6883	6876	20222	17466	1077	5627	1611	4883
175	XG-5	3	474	127236	9268	15851	195499	237948	17305	41110	5807	5968	19151	15839	1121	4786	1215	4674
176	XG-5	3	2055	125924	11873	3687	181025	232010	16285	42302	5983	5539	54899	761	766	3009	314	1074
177	XG-5	3	977	130174	13441	20234	173965	219660	16534	39798	5584	6900	38204	15982	666	6000	1514	6099
178	XG-5	4	25873	92933	1377	533	114334	209838	19186	62942	5129	1596	133355	2577		24		7170
179	XG-5	4	21286	102094	2174	721	124363	223002	20233	67310	5121	1845	106424	1898	105	256	77	6949
180	XG-5	4	2812	126188	3086	2048	162987	281104	24613	77299	7513	3105	22196	718	412	808	236	2293
181	XG-5	4	1048	127146	8681	2621	155524	269129	23609	74747	7054	3022	32392	1118	629	552	598	3273
182	XG-5	4	3040	125526	6309	4093	127836	255169	26329	95336	15034	9809	34155	1235	1004	2242	323	3395
183	XG-5	4	3252	125060	6282	4655	125986	254170	26515	94828	15194	9238	35256	1292	638	2407	274	3655
184	XG-5	4	7874	117637	405	2287	133795	266160	27256	94116	12923	7390	36547	1254	489	973	299	3586
185	XG-5	4	4612	123351	3844	1280	112963	265467	30042	112289	13784	5568	34087	700	311	445	180	3303

TABLE A2
(continued)

spot#	sample	grain	Si	P	Ca	Y	La	Ce	Pr	Nd	Sm	Gd	Th	U	Tb	Dy	Er	Pb avg
186	XG-6	10	10459	113649	4491	62	94127	238078	29844	115966	14309	3970	65825	975	723	216		6276
187	XG-6	10	13778	107685	3705		84339	228785	29618	121683	12173	1612	81425	1321	185		134	7397
188	XG-6	10	6182	119022	3410		102043	257460	31400	123688	14357	3540	41325	646			130	3937
189	XG-6	10	6919	117909	6626	391	100135	234238	27879	115367	19285	8615	55871	1502	511	364		5497
190	XG-6	10	2600	125383	7087	6147	109838	240905	28262	106046	20701	14790	33109	3218	1076	3195	327	3948
191	XG-6	6	12847	108111	3595		86188	229603	29988	121007	12723	1847	75333	1302			104	6668
192	XG-6	6	2924	123985	5605	2549	110128	242161	28428	109490	21180	14446	31745	1947	1242	1855	86	3421
193	XG-6	6	3258	124201	6244	1160	109486	247747	28356	109822	20681	11607	35937	1516	821	1023	101	3763
194	XG-6	6	10521	115050	3415		91579	239752	29549	119744	13047	2989	64208	850	257	31	297	5706
195	XG-6	6	4883	123175	3894	930	106053	246525	29192	118293	19352	10256	36092	995	210	871		3525
196	XG-6	6	1985	127076	6705	6897	111961	239203	27647	103997	20173	16742	28888	3442	1404	4440	155	3616
197	XG-6	6	9174	113549	3299		93576	244824	30092	119552	13108	3549	56411	1054		37		5410
198	XG-6	6	12994	108619	3581		83849	228943	30241	121571	11899	2613	75676	1068	344		9	6879
199	XG-6	6	6030	118496	4455	770	95679	247737	30443	120142	16287	5520	44566	948	399	217	203	4487
200	XG-6	7	1543	128216	8238	6516	110574	239635	26722	103989	19945	15791	33058	2879	1351	3792	282	3768
201	XG-6	7	1485	128946	8176	6849	113046	239101	27835	104219	19888	16071	32313	2754	1143	3985	414	3781
202	XG-6	7	4601	122183	4111	757	102711	259095	31909	118213	15577	5215	35724	963	357	267	119	3595
203	XG-6	7	5942	122127	3901		100165	255822	32104	122719	16832	3702	41123	621	852		81	4113
204	XG-6	7	6914	121764	5559	828	96232	245515	30110	118321	16250	6737	51668	957	347	637	167	5037
205	XG-6	7	8889	115819	1298	1048	98868	247697	30180	121781	18114	7900	53688	641	121	597		374
206	XG-6	7	6902	118509	2183	548	100773	251021	31678	125927	17270	6465	45886	617	627	216	148	278
207	XG-2	1	22854	97282	2848	1409	122678	218431	19259	59478	4399	2490	117860	2541	332	401	1	10958
208	XG-2	1	22168	99579	2964	1366	126002	217505	19201	58895	4591	1848	114348	2469	249	428		10298
209	XG-2	1	23134	95559	2904	1373	121033	216942	19173	59110	4970	2031	120446	2671	316	518	2	10623
210	XG-2	1	26159	91625	3162	1332	117271	206150	19017	53291	4862	1652	136165	2327	139	245	42	8010
211	XG-2	1	25695	91014	2853	1247	117693	208167	18195	54854	4452	2099	136064	2276	13	233	109	7855
212	XG-2	1	40928	69065	5604	1002	99327	144967	13948	42851	3631	1522	215710	4432	68	371	91	6025
213	XG-2	1	50893	54911	3964	819	80798	117966	11394	37130	3642	1937	263616	5061	60	501		8290
214	XG-7	1	4797	121124	6005	3796	139539	286835	27448	86221	8743	3424	18887	291	122	1020	417	27
215	XG-7	1	4993	121168	5327	3617	138900	287477	27491	87921	8642	4192	20168	28	203	995	148	41
216	XG-7	1	4488	122237	5112	3297	141742	288044	27012	86698	8951	3671	18483	205	321	1051	169	79
217	XG-7	1	3699	124067	4832	2842	152226	292950	27574	82297	8351	3274	10906	236	375	848	115	11
218	XG-7	1	3863	123267	4630	3040	147520	291410	27086	83632	7549	3378	12720		255	923	475	35
219	XG-7	1	3750	122484	4854	2941	148762	289830	27152	83881	7199	3808	11954	13	53	940	383	46

References

Aleinikoff, J. N., Schenck, W. S., Plank, M. O., Srogi, L., Fanning, C. M., Kamo, S. L., and Bosbyshell, H., 2006, Deciphering igneous and metamorphic events in high-grade rocks of the Wilmington Complex, Delaware: Morphology, cathodoluminescence and backscattered electron zoning, and SHRIMP U-Pb geochronology of zircon and monazite: Geological Society of America Bulletin, v. 118, p. 39–64, http://dx.doi.org/10.1130/B25659.1

Andersen, T., 2002, Correction of common lead in U-Pb analyses that do not report ^{204}Pb: Chemical Geology, v. 192, n. 1–2, p. 59–79, http://dx.doi.org/10.1016/S0009-2541(02)00195-X

Anderson, J. L., 1989, Proterozoic anorogenic granites of the southwestern United States, *in* Jenney, J. P., and Reynolds, S. J., editors, Geological evolution of Arizona: Arizona Geological Society Digest, v. 17, p. 211–238.

Ayers, J. C., Dunkle, S., Gao, S., and Miller, C. F., 2002, Constraints on timing of peak and retrograde metamorphism in the Dabie Shan Ultrahigh-Pressure Metamorphic Belt, east-central China, using U-Th-Pb dating of zircon and monazite: Chemical Geology, v. 186, n. 3–4, p. 315–331, http://dx.doi.org/10.1016/S0009-2541(02)00008-6

Ayers, J. C., Loflin, M., Miller, C. F., Barton, M. D., and Coath, C., 2004, Dating fluid infiltration using monazite, *in* Wanty, R. B., and Seal, R. R., II, editors, Proceedings of the Eleventh International Symposium on Water-Rock Interaction: Saratoga Springs, New York, A. A. Balkema Publishers, p. 247–251.

Ayers, J. C., Loflin, M., Miller, C. F., Barton, M. D., and Coath, C. D., 2006, In situ oxygen isotope analysis of monazite as a monitor of fluid infiltration during contact metamorphism: Birch Creek Pluton aureole, White Mountains, eastern California: Geology, v. 34, n. 8, p. 653–656, http://dx.doi.org/10.1130/G22185.1

Bachl, C. A., Miller, C. F., Miller, J. S., and Faulds, J. E., 2001, Construction of a pluton: Evidence from an exposed cross section of the Searchlight pluton, Eldorado Mountains, Nevada: Geological Society of America Bulletin, v. 113, n. 9, p. 1213–1228, http://dx.doi.org/10.1130/0016-7606(2001)113⟨1213:COAPEF⟩2.0.CO;2

Bennett, V. C., and DePaolo, D. J., 1987, Proterozoic crustal history of the Western United States as determined by neodymium isotopic mapping; with Supplementary Data 87-30: Geological Society of America Bulletin, v. 99, n. 5, p. 674–685, http://dx.doi.org/10.1130/0016-7606(1987)99⟨674:PCHOTW⟩2.0.CO;2

Bosse, V., Boulvais, P., Gautier, P., Tiepolo, M., Ruffet, G., Devidal, J. L., Cherneva, Z., Gerdjikov, I., and Paquette, J. L., 2009, Fluid-induced disturbance of the monazite Th-Pb chronometer: In situ dating and element mapping in pegmatites from the Rhodope (Greece, Bulgaria): Chemical Geology, v. 261, n. 3–4, p. 286–302, http://dx.doi.org/10.1016/j.chemgeo.2008.10.025

Boynton, W. V., 1984, Geochemistry of the rare earth elements: meteorite studies, *in* Henderson, P., editor, Rare Earth Element Geochemistry: Elsevier, Developments in Geochemistry, v. 2, p. 63–114.

Brimhall, G. H., and Crerar, D. A., 1987, Ore fluids; magmatic to supergene, *in* Carmichael, I. S. E., and Eugster, H. P., editors, Thermodynamic modeling of geological materials; minerals, fluids and melts: Reviews in Mineralogy, v. 17, p. 235–321.

Bryant, D. L., Ayers, J. C., Gao, S., Miller, C. F., and Zhang, H., 2004, Geochemical, Age, and Isotopic Constraints on the Location of the Sino-Korean/Yangtze Suture and Evolution of the Northern Dabie Complex, East Central China: Geological Society of America Bulletin, v. 116, n. 5–6, p. 698–717, http://dx.doi.org/10.1130/B25302.2

Callaghan, E., 1939, Geology of the Searchlight District, Clark County, Nevada: U.S. Geological Survey Bulletin 906-D, p. 135–188.

Carson, C. J., Ague, J. J., Grove, M., Coath, C. D., and Harrison, T. M., 2002, U-Pb isotopic behaviour of zircon during upper-amphibolite facies fluid infiltration in the Napier Complex, east Antarctica: Earth and Planetary Science Letters, v. 199, n. 3–4, p. 287–310, http://dx.doi.org/10.1016/S0012-821X(02)00565-4

Cates, N. L., Miller, J. S., Miller, C. F., Wooden, J. L., Ericksen, S., and Means, M., 2003, Longevity of plutonic systems; SHRIMP evidence from Aztec Wash and Searchlight plutons, Nevada: Geological Society of America, Abstracts with Programs, v. 35, p. 63.

Cherniak, D. J., Watson, E. B., Grove, M., and Harrison, T. M., 2004, Pb diffusion in monazite: a combined RBS/SIMS study: Geochimica et Cosmochimica Acta, v. 68, n. 4, p. 829–840, http://dx.doi.org/10.1016/j.gca.2003.07.012

Clayton, R. N., and Mayeda, T. K., 1963, The use of bromine pentafluoride in the extraction of oxygen from oxides and silicates for isotopic analysis: Geochimica et Cosmochimica Acta, v. 27, p. 43–52, http://dx.doi.org/10.1016/0016-7037(63)90071-1

Colombini, L. L., Miller, C. F., Gualda, G. A. R., Wooden, J. L., and Miller, J. S., 2011, Sphene and zircon in the Highland Range volcanic sequence (Miocene, southern Nevada, USA): elemental partitioning, phase relations, and influence on evolution of silicic magma: Mineralogy and Petrology, v. 102, n. 1–4, p. 29–50, http://dx.doi.org/10.1007/s00710-011-0177-3

Copeland, P., Parrish, R. R., and Harrison, T. M., 1988, Identification of inherited radiogenic Pb in monazite and its implications for U-Pb systematics: Nature, v. 333, p. 760–763, http://dx.doi.org/10.1038/333760a0

Crombie, S. A., ms, 2006, Monazite alteration in the Searchlight Contact Metamorphic Aureole, Southern Nevada: Nashville, Tennessee, Vanderbilt University, Master of Science degree, 65 p.

Engi, M., Cheburkin, A. K., and Koeppel, V., 2002, Nondestructive chemical dating of young monazite using XRF: 1, Design of a mini-probe, age data for samples from the Central Alps, and comparison to U-Pb (TIMS) data: Chemical Geology, v. 191, n. 1–3, p. 225–241, http://dx.doi.org/10.1016/S0009-2541(02)00158-4

Faulds, J. E., Geissman, J. W., and Mawer, C. K., 1990, Structural development of a major extensional accommodation zone in the Basin and Range Province, northwestern Arizona and southern Nevada: implications for kinematic models of continental extension: Geological Society of America Memoirs, v. 176, p. 37–76.

Faulds, J. E., Feuerbach, D. L., Miller, C. F., and Smith, E. I., 2001, Cenozoic evolution of the northern Colorado River extensional corridor, southern Nevada and northwest Arizona: Utah Geological Association Publication 30–Pacific Section American Association of Petroleum Geologists Publication, v. GB78, p. 239–271.

Faulds, J. E., Olson, E. L., Harlan, S. S., and McIntosh, W. C., 2002, Miocene extension and fault-related folding in the Highland Range, southern Nevada: A three-dimensional perspective: Journal of Structural Geology, v. 24, n. 4, p. 861–886, http://dx.doi.org/10.1016/S0191-8141(01)00116-X

Faulds, J. E., Miller, C. F., Miller, J. S., and Ludington, S., 2008, The Searchlight magmatic system, southern Nevada and northwest Arizona: Anatomy and evolution of a pre- to syn-extensional putonic-volcanic system in the highly extended Colorado River extensional corridor: Geological Society of America Abstracts with Programs, v. 40, n. 1, p. 85.

Getty, S. R., and Gromet, L. P., 1992, Geochronological constraints on ductile deformation, crustal extension, and doming about a basement-cover boundary, New England Appalachians: American Journal of Science, v. 292, n. 6, p. 359–397, http://dx.doi.org/10.2475/ajs.292.6.359

Gordon, S. M., Grove, M., Whitney, D. L., Schmitt, A. K., and Teyssier, C., 2009, Time-temperature-fluid evolution of migmatite dome crystallization: Coupled U-Pb age, Ti thermometry, and O isotopic ion microprobe depth profiling of zircon and monazite: Chemical Geology, v. 262, n. 3–4, p. 186–201, http://dx.doi.org/10.1016/j.chemgeo.2009.01.018

Griffin, W., Powell, W., Pearson, N., and O'Reilly, S., 2008, GLITTER: data reduction software for laser ablation ICP-MS: Laser Ablation-ICP-MS in the Earth Sciences, v. 40, p. 204–207.

Hammond, J. G., and Wooden, J. L., 1990, Isotopic constraints on the petrogenesis of Proterozoic diabase in southwestern USA: Proceedings of the International Dyke Conference, v. 2, p. 145–156.

Harlov, D. E., and Hetherington, C. J., 2010, Partial high-grade alteration of monazite using alkali-bearing fluids: Experiment and nature: American Mineralogist, v. 95, n. 7, p. 1105–1108, http://dx.doi.org/10.2138/am.2010.3525

Harlov, D. E., Wirth, R., and Hetherington, C. J., 2011, Fluid-mediated partial alteration in monazite: the role of coupled dissolution-reprecipitation in element redistribution and mass transfer: Contributions to Mineralogy and Petrology, v. 162, n. 2, p. 329–348, http://dx.doi.org/10.1007/s00410-010-0599-7

Harrison, T. M., Grove, M., McKeegan, K. D., Coath, C. D., Lovera, O. M., and Le Fort, P., 1999, Origin and episodic emplacement of the Manaslu Intrusive Complex, central Himalaya.: Journal of Petrology, v. 40, n. 1, p. 3–19, http://dx.doi.org/10.1093/petroj/40.1.3

Harrison, T. M., Catlos, E. J., and Montel, J.-M., 2002, U-Th-Pb dating of phosphate minerals, *in* Kohn, M. J., Rakovan, J., and Hughes, J. M., editors, Phosphates: geochemical, geobiological, and materials importance: Reviews in Mineralogy and Geochemistry, v. 48, p. 524–558, http://dx.doi.org/10.2138/rmg.2002.48.14

Hawkins, D. P., and Bowring, S. A., 1997, U-Pb systematics of monazite and xenotime: case studies from the Paleoproterozoic of the Grand Canyon, Arizona: Contributions to Mineralogy and Petrology, v. 127, n. 1–2, p. 87–103, http://dx.doi.org/10.1007/s004100050267

Kapp, J. D. A., Miller, C. F., and Miller, J. S., 2002, Ireteba Pluton, Eldorado Mountains, Nevada: Late, Deep-Source, Peraluminous Magmatism in the Cordilleran Interior: The Journal of Geology, v. 110, n. 6, p. 649–669, http://dx.doi.org/10.1086/342864

Kingsbury, J. A., Miller, C. F., Wooden, J. L., and Harrison, T. M., 1993, Monazite paragenesis and U-Pb systematics in rocks of the eastern Mojave Desert, California, U.S.A.: Implications for thermochronometry: Chemical Geology, v. 110, n. 1–3, p. 147–168, http://dx.doi.org/10.1016/0009-2541(93)90251-D

Lledo, H., and Cline, J. S., 2008, The Searchlight mining district; linking low sulfidation epithermal mineralization with an underlying granitic pluton using S and Pb isotopes: Geological Society of America, Abstracts with Programs, v. 40, p. 51.

Loflin, M. I., ms, 2002, Monazite as a Tracer of Fluid Infiltration Associated with Contact Metamorphism: Nashville, Tennessee, Vanderbilt University, Master of Science degree, 65 p.

Ludington, S., Castor, S. B., Faulds, J. E., and Flynn, K. S., 2005, The Searchlight District, Nevada; oxidized, but when?: Geological Society of America, Abstracts with Programs, v. 37, p. 516–517.

Ludwig, K. R., 2000, Users Manual for Isoplot/Ex: A Geochronoligical Toolkit for Microsoft Excel: Berkeley Geochronology Center Special Publication, 53 p.

Mathieu, R., Zetterstrom, L., Cuney, M., Gauthier-Lafaye, F., and Hidaka, H., 2001, Alteration of monazite and zircon and lead migration as geochemical tracers of fluid paleocirculations around the Oklo-Okélobondo and Bangombé natural nuclear reaction zones (Franceville Basin, Gabon): Chemical Geology, v. 171, n. 3–4, p. 147–171, http://dx.doi.org/10.1016/S0009-2541(00)00245-X

McFarlane, C. R. M., and Harrison, T. M., 2006, Pb-diffusion in monazite: Constraints from a high-*T* contact aureole setting: Earth and Planetary Science Letters, v. 250, n. 1–2, p. 376–384, http://dx.doi.org/10.1016/j.epsl.2006.06.050

Means, M., Miller, J., Miller, C., Cates, N., Wooden, J., and Ericksen, S., 2003, Mafic injection into a nearly frozen magma chamber: failed (?) rejuvenation and local hybridization in the Searchlight pluton, Eldorado Mountains, Nevada (USA): American Geophysical Union, Eos, Transactions, v. 84, p. F1630–1631.

Miller, C. F., and Wooden, J. L., 1994, Anatexis, hybridization and the modification of ancient crust: Mesozoic plutonism in the Old Woman Mountains area, California: Lithos, v. 32, n. 1–2, p. 111–133, http://dx.doi.org/10.1016/0024-4937(94)90025-6

Miller, J. S., Cates, N. L., Miller, C. F., Wooden, J., Means, M. A., and Ericksen, S., 2003, Magmatic

construction and duration of solidification of Searchlight pluton, Eldorado Mountains, Nevada (USA): American Geophysical Union, Eos, Transactions, v. 84, p. F1630.

Paces, J. B., and Miller, J. D., Jr., 1993, Precise U-Pb Ages of Duluth Complex and Related Mafic Intrusions, Northeastern Minnesota: Geochronological Insights to Physical, Petrogenetic, Paleomagnetic, and Tectonomagmatic Processes Associated With the 1.1 Ga Midcontinent Rift System: Journal of Geophysical Research, v. 98, n. B8, p. 13997–14013, http://dx.doi.org/10.1029/93JB01159

Paquette, J. L., and Tiepolo, M., 2007, High resolution (5 μm) U-Th-Pb isotope dating of monazite with excimer laser ablation (ELA)-ICPMS: Chemical Geology, v. 240, n. 3–4, p. 222–237, http://dx.doi.org/10.1016/j.chemgeo.2007.02.014

Perrault, D. S., ms, 2006, Giant country rock blocks within Searchlight pluton, southern Nevada: Nashville, Tennessee, Vanderbilt University, Master's Thesis, 113 p.

Poitrasson, F., Chenery, S., and Shepherd, T. J., 2000, Electron microprobe and LA-ICP-MS study of monazite hydrothermal alteration: Implications for U-Th-Pb geochronology and nuclear ceramics: Geochimica et Cosmochimica Acta, v. 64, n. 19, p. 3283–3297, http://dx.doi.org/10.1016/S0016-7037(00)00433-6

Poitrasson, F., Oelkers, E., Schott, J., and Montel, J.-M., 2004, Experimental determination of synthetic $NdPO_4$ monazite end-member solubility in water from 21 °C to 300 °C: implications for rare earth element mobility in crustal fluids: Geochimica et Cosmochimica Acta, v. 68, n. 10, p. 2207–2221, http://dx.doi.org/10.1016/j.gca.2003.12.010

Pyle, J. M., Spear, F. S., Wark, D. A., Daniel, C. G., and Storm, L. C., 2005, Contributions to precision and accuracy of monazite microprobe ages: American Mineralogist, v. 90, n. 4, p. 547–577, http://dx.doi.org/10.2138/am.2005.1340

Quidelleur, X., Grove, M., Lovera, O. M., Harrison, T. M., Yin, A., and Ryerson, F. J., 1997, Thermal evolution and slip history of the Renbu Zedong thrust, southeastern Tibet.: Journal of Geophysical Research, v. 102, n. B2, p. 2659–2679, http://dx.doi.org/10.1029/96JB02483

Rasmussen, B., and Fletcher, I. R., 2002, Indirect dating of mafic intrusions by SHRIMP U-Pb analysis of monazite in contact metamorphosed shale: an example from the Palaeoproterozoic Capricorn Orogen, Western Australia: Earth and Planetary Science Letters, v. 197, n. 3–4, p. 287–299, http://dx.doi.org/10.1016/S0012-821X(02)00501-0

Rasmussen, B., Fletcher, I. R., and McNaughton, N. J., 2001, Dating low-grade metamorphic events by SHRIMP U-Pb analysis of monazite in shales: Geology, v. 29, n. 10, p. 963–966, http://dx.doi.org/10.1130/0091-7613(2001)029⟨0963:DLGMEB⟩2.0.CO;2

Rasmussen, B., Sheppard, S., and Fletcher, I. R., 2006, Testing ore deposit models using in situ U-Pb geochronology of hydrothermal monazite: Paleoproterozoic gold mineralization in northern Australia: Geology, v. 34, n. 2, p. 77–80, http://dx.doi.org/10.1130/G22058.1

Rasmussen, B., Fletcher, I. R., Muhling, J. R., Mueller, A. G., and Hall, G. C., 2007, Bushveld-aged fluid flow, peak metamorphism, and gold mobilization in the Witwatersrand basin, South Africa: Constraints from in situ SHRIMP U-Pb dating of monazite and xenotime: Geology, v. 35, n. 10, p. 931–934, http://dx.doi.org/10.1130/G23588A.1

Smith, H. A., and Barreiro, B., 1990, Monazite U-Pb dating of staurolite grade metamorphism in pelitic schists: Contributions to Mineralogy and Petrology, v. 105, n. 5, p. 602–15, http://dx.doi.org/10.1007/BF00302498

Spear, F. S., and Pyle, J. M., 2002, Apatite, monazite, and xenotime in metamorphic rocks, *in* Kohn, M. J., Rakovan, J., and Hughes, J. M., editors, Phosphates; geochemical, geobiological, and materials importance: Reviews in Mineralogy and Geochemistry, v. 48, p. 293–335, http://dx.doi.org/10.2138/rmg.2002.48.7

Strickland, A., Wooden, J. L., Mattinson, C. G., Ushikubo, T., Miller, D. M., and Valley, J. W., 2013, Proterozoic evolution of the Mojave crustal province as preserved in the Ivanpah Mountains, southeastern California: Precambrian Research, v. 224, p. 222–241, http://dx.doi.org/10.1016/j.precamres.2012.09.006

Sun, S.-s., and McDonough, W. F., 1989, Chemical and isotopic systematics of oceanic basalts: implications for mantle composition and processes: Geological Society, London, Special Publications, v. 42, p. 313–345, http://dx.doi.org/10.1144/GSL.SP.1989.042.01.19

Townsend, K. J., ms, 1999, Monazite Paragenesis in the Ireteba Granite, Southern Nevada: Geochronological Implications: Nashville, Tennessee, Vanderbilt University, Masters Thesis, 75 p.

Townsend, K. J., Miller, C. F., D'Andrea, J. L., Ayers, J. C., Harrison, T. M., and Coath, C. D., 2000, Low temperature replacement of monazite in the Ireteba granite, Southern Nevada: geochronological implications: Chemical Geology, v. 172, n. 1–2, p. 95–112, http://dx.doi.org/10.1016/S0009-2541(00)00238-2

van Achterbergh, E., Ryan, C. G., Jackson, S. E., and Griffin, W. L., 2001, Data reduction software for LA-ICP-MS, *in* Sylvester, P. J., editor, Laser-ablation-ICPMS in the earth sciences; principles and applications: Ottawa, Ontario, Mineralogical Association of Canada, Short Course Series, n. 29, p. 239–243.

Wiedenbeck, M., Hanchar, J. M., Peck, W. H., Sylvester, P., Valley, J., Whitehouse, M., Kronz, A., Morishita, Y., Nasdala, L., Fiebig, J., Franchi, I., Girard, J.-P., Greenwood, R. C., Hinton, R., Kita, N., Mason, P. R. D., Norman, M., Ogasawara, M., Piccoli, P. M., Rhede, D., Satoh, H., Schulz-Dobrick, B., Skår, O., Spicuzza, M. J., Terada, K., Tindle, A., Togashi, S., Vennemann, T., Xie, Q., and Zheng, Y.-F., 2004, Further characterization of the 91500 zircon crystal: Geostandards and Geoanalytical Research, v. 28, n. 1, p. 9–39, http://dx.doi.org/10.1111/j.1751-908X.2004.tb01041.x

Williams, M. L., Jercinovic, M. J., and Terry, M. P., 1999, Age mapping and dating of monazite on the electron microprobe: Deconvoluting multistage tectonic: Geology, v. 27, n. 11, p. 1023, http://dx.doi.org/10.1130/0091-7613(1999)027⟨1023:AMADOM⟩2.3.CO;2

Williams, M. L., Jercinovic, M. J., Harlov, D. E., Budzyn, B., and Hetherington, C. J., 2011, Resetting monazite ages during fluid-related alteration: Chemical Geology, v. 283, n. 3–4, p. 218–225, http://dx.doi.org/10.1016/j.chemgeo.2011.01.019

Wooden, J. L., and Miller, D. M., 1990, Chronologic and isotopic framework for early Proterozoic crustal evolution in the eastern Mojave Desert region, SE California: Journal of Geophysical Research, v. 95, n. B12, p. 20,133–20,146, http://dx.doi.org/10.1029/JB095iB12p20133

Zhu, X. K., and O'Nions, R. K., 1999, Zonation of monazite in metamorphic rocks and its implications for high temperature thermochronology: a case study from the Lewisian terrain: Earth and Planetary Science Letters, v. 171, n. 2, p. 209–220, http://dx.doi.org/10.1016/S0012-821X(99)00146-6